Fock-space perturbed relativistic coupled-cluster theory for electric dipole polarizability of one-valence atomic systems: Application to Al and In

Ravi Kumar,[1] D. Angom,[2,3] and B. K. Mani[1,*]

[1]*Department of Physics, Indian Institute of Technology, Hauz Khas, New Delhi 110016, India*
[2]*Department of Physics, Manipur University, Canchipur 795003, Manipur, India*
[3]*Physical Research Laboratory, Ahmedabad 380009, Gujarat, India*

We have developed a Fock-space relativistic coupled-cluster theory-based method for the calculation of electric dipole polarizability of one-valence atoms and ions. We employ this method to compute the ground-state and spin-orbit coupled excited state electric dipole polarizability of Al and In. To check the quality of many-electron wave functions, we also compute the excitation energies of some low-lying states of Al and In. The effects of the Breit interaction and QED corrections from the Uehling potential and the self-energy are included to improve the accuracy of α further. Our recommended values of the ground-state α for both atoms are in good agreement with the previous theoretical results. From our computations, we find that more than 65% of contributions come from the dipolar mixing of $3p(5p)$ with $3d(5d)$ and $4s(6s)$ electrons for Al(In). The largest Breit and QED contributions are found to be 1.3% and 0.6%, respectively.

I. INTRODUCTION

Group-13 elements are promising candidates for accurate optical atomic clocks as they offer low fractional frequency errors [1–5]. Recent experiments [6,7] on Al$^+$ optical atomic clock have achieved a low fractional frequency error of 9.4×10^{-19} [6,7], which is, perhaps, the most accurate clock in existence today. The electric dipole polarizability, α, of an atom or ion is a key parameter in estimating the accuracy of an atomic clock. It is used to estimate the blackbody radiation shift, one of the dominant environment-induced frequency shifts, in the transition frequencies of atoms and ions due to the ac Stark effect. Since the measurement of α for individual states is nontrivial [8], accurate values from precision theory calculations play a crucial role in the development of new frequency and time standards for atomic clocks. The other potential implications of α include discrete symmetry violations in atoms and ions [9,10], condensates of dilute atomic gases [11–13], high-harmonic generation and ultrafast processes [14–17], and the search for variation in the fundamental constants [18,19].

In this work, we have employed a Fock-space perturbed relativistic coupled-cluster theory to compute the properties of one-valence atomic systems in the external perturbations. We employ this method to compute the α for the ground state, $^2P_{1/2}$, and the spin-orbit (SO)-split excited state, $^2P_{3/2}$, of Al and In. The reason for choosing Al and In over the other group-13 elements is that previous theoretical and experimental works have studied both elements extensively. This is a basic and essential requirement to assess the potential applications and accuracy of our method. In the literature, α for $^2P_{1/2}$

and $^2P_{3/2}$ states of Al and In have been calculated using different methods [20–25], including the coupled-cluster based methods like ours. One common trend in the reported data is, however, a large variation in the α values. For example, for the $^2P_{1/2}$ state of Al, there is a difference of $\approx 10\%$ in the smallest [20] and the largest [25] reported α values. The same trend is also observed in the experimental values [26–29]. The experiment [27] reports $\approx 20\%$ larger α than Ref. [26] for Al. It is to be emphasized that, unlike the closed-shell atomic systems, calculation of α for an open-shell system is a challenging task and requires the inclusion of *core-core*, *core-valence*, and *valence-valence* electrons correlations to the highest level of accuracy. Moreover, the inclusion of correlation effects from Breit interaction and QED corrections and the large basis sets are essential to tune the accuracy further. The aim of the present work is to fill this gap. We aim to develop a Fock-space relativistic coupled-cluster theory-based method to accurately account for an external perturbation in the properties calculation of one-valence atomic systems, compute the accurate value of α for Al and In, and quantify the various electron correlation effects embedded in the α of Al and In.

To test the accuracy of the wave functions, we have calculated excitation energies of a few low-lying states of Al and In using RCC theory. RCC is one of the most powerful many-body theories for atomic structure calculations. It accounts for the electron correlation to all orders of residual Coulomb interaction and has been used to calculate a plethora of properties in atomic systems. The implementation of such a theory and a FORTRAN code for the properties' calculations of closed-shell and one-valence atomic systems without external perturbation is reported in our previous work [30]. For the properties' calculation in the presence of external perturbation, we reported a perturbed relativistic coupled-cluster (PRCC) theory for closed-shell in [31,32] and references

*[*]bkmani@physics.iitd.ac.in

032801-1

therein. One of the key merits of PRCC is that it does not employ the sum-over-state [33,34] approach to incorporate the effects of a perturbation. The summation over all the possible intermediate states is subsumed in the perturbed cluster operators. Due to important prospects associated with α, it has been computed using a variety of other many-body methods in the literature. The review article by Mitroy *et al.* [35] provides a summary of α for several atoms and ions computed using different methods. The other reference which we found very useful is Schwerdtfeger's updated table of α for neutral atoms [36]. The table provides an exhaustive list of references on experimental and theoretical values of α for several neutral atoms.

This paper is organized into five further sections. In Sec. II we discuss the RCC and PRCC theories for one-valence atomic systems where we derive the PRCC equations and discuss in detail the contributing diagrams to each term. In Sec. III we discuss the calculation of α using PRCC theory. Here we provide some dominant diagrams contributing to α. The basis set convergence and other calculational details are discussed in Sec. IV. In Sec. V we analyze and present our results of excitation energy and dipole polarizability. Unless stated otherwise, all results and equations presented in this paper are in atomic units ($\hbar = m_e = e = 1/4\pi\epsilon_0 = 1$).

II. METHODOLOGY

A. One-valence RCC theory

The many-electron ground state wave function of a one-valence atom or ion in the RCC theory is expressed as

$$|\Psi_v\rangle = e^{(T^{(0)}+S^{(0)})} |\Phi_v\rangle, \tag{1}$$

where $|\Phi_v\rangle$ is the one-valence Dirac-Fock (DF) reference state and is obtained by adding an electron to the closed-shell reference state, $|\Phi_v\rangle = a_v^\dagger|\Phi_0\rangle$. The operators $T^{(0)}$ and $S^{(0)}$ are the coupled cluster (CC) operators which act within the Hilbert spaces of the closed-shell and open-shell systems, respectively. The ground state $|\Psi_v\rangle$ is the solution of the eigenvalue equation

$$H^{\text{DCB}}|\Psi_v\rangle = E_v|\Psi_v\rangle, \tag{2}$$

where H^{DCB} is the Dirac-Coulomb-Breit no-virtual-pair Hamiltonian and E_v is the exact energy of the one-valence system. For an atom with N electrons, H^{DCB} is

$$H^{\text{DCB}} = \sum_{i=1}^{N}[c\boldsymbol{\alpha}_i \cdot \mathbf{p}_i + (\beta_i - 1)c^2 - V_N(r_i)]$$
$$+ \sum_{i<j}\left[\frac{1}{r_{ij}} + g^{\text{B}}(r_{ij})\right], \tag{3}$$

where $\boldsymbol{\alpha}$ and β are the Dirac matrices and $V_N(r_i)$ is the nuclear potential. The last two terms, $1/r_{ij}$ and $g^{\text{B}}(r_{ij})$, are the Coulomb and Breit interactions, respectively. For Breit interaction, we employ the expression [37]

$$g^{\text{B}}(r_{12}) = -\frac{1}{2r_{12}}\left[\boldsymbol{\alpha}_1 \cdot \boldsymbol{\alpha}_2 + \frac{(\boldsymbol{\alpha}_1 \cdot \mathbf{r}_{12})(\boldsymbol{\alpha}_2 \cdot \mathbf{r}_{12})}{r_{12}^2}\right]. \tag{4}$$

The effects of the negative-energy continuum states are avoided by employing a kinetically balanced finite Gaussian basis [38,39].

In the RCC theory, the single and double excitations incorporate most of the electron correlation effects and provide a good description of the properties. Therefore, we can approximate $T^{(0)} = T_1^{(0)} + T_2^{(0)}$ and $S^{(0)} = S_1^{(0)} + S_2^{(0)}$, which is referred to as the coupled cluster with single and double (CCSD) approximation. These operators in the second quantized notation are

$$T_1^{(0)} = \sum_{ap} t_a^p a_p^\dagger a_a, \quad \text{and} \quad T_2^{(0)} = \frac{1}{2!}\sum_{abpq} t_{ab}^{pq} a_p^\dagger a_q^\dagger a_b a_a, \tag{5a}$$

$$S_1^{(0)} = \sum_{p} s_v^p a_p^\dagger a_v, \quad \text{and} \quad S_2^{(0)} = \sum_{apq} s_{va}^{pq} a_p^\dagger a_q^\dagger a_a a_v. \tag{5b}$$

Here the indices $ab\ldots$ and $pq\ldots$ represent the core and virtual orbitals, respectively, and $t_{\cdots}^{\cdots}$ and $s_{\cdots}^{\cdots}$ are the cluster amplitudes of the T and S operators, respectively. These closed-shell and one-valence operators are obtained by solving a set of coupled nonlinear equations, and details are discussed in our previous works [30,40,41]. In Ref. [30] we have provided descriptions of the computational implementation of RCC theory for the properties calculations of the closed-shell and one-valence systems without an external perturbation.

B. One-valence PRCC theory

In the presence of an external perturbation, the wave function and the energy of the system are modified. For the electric dipole polarizability, the perturbation is due to the interaction between the external electric field $\mathbf{E}_{\text{ext}}$ and the induced electric dipole moment of the system $\mathbf{D}$. The interaction Hamiltonian is $H_1 = -\mathbf{D} \cdot \mathbf{E}_{\text{ext}}$. We refer the modified eigenstate as the perturbed eigenstate, $|\tilde{\Psi}_v\rangle$, and the modified energy as the perturbed energy, $\tilde{E}_v$. In the PRCC theory, $|\tilde{\Psi}_v\rangle$ is expressed as

$$|\tilde{\Psi}_v\rangle = e^{T^{(0)}}[1 + \lambda\mathbf{T}^{(1)} \cdot \mathbf{E}_{\text{ext}}]$$
$$\times [1 + S^{(0)} + \lambda\mathbf{S}^{(1)} \cdot \mathbf{E}_{\text{ext}}]|\Phi_v\rangle, \tag{6}$$

where λ is the perturbation parameter. The operators $\mathbf{T}^{(1)}$ and $\mathbf{S}^{(1)}$ are referred to as the perturbed closed-shell and one-valence cluster operators, respectively, and both are rank one operators. The operator $\mathbf{T}^{(1)}$ is obtained by solving a set of coupled perturbed equations within the Hilbert space of the occupied electrons. The details for its tensor representation and the PRCC equations are discussed in our previous works on the dipole polarizability of the closed-shell atomic systems [31,42]. Here we discuss only the tensor representation and PRCC equations of the open-shell cluster operator $\mathbf{S}^{(1)}$.

Similar to the case of $T^{(0)}$ and $S^{(0)}$ operators, in the CCSD approximation, we take $\mathbf{S}^{(1)} = S_1^{(1)} + S_2^{(1)}$. These are in the second quantized notations,

$$\mathbf{S}_1^{(1)} = \sum_{p} \xi_v^p \mathbf{C}_1(\hat{r}) a_p^\dagger a_v, \tag{7a}$$

$$\mathbf{S}_2^{(1)} = \sum_{apq}\sum_{lk} \xi_{va}^{pq}(l,k)\mathbf{C}_l(\hat{r}_1)\mathbf{C}_k(\hat{r}_2) a_p^\dagger a_q^\dagger a_a a_v. \tag{7b}$$
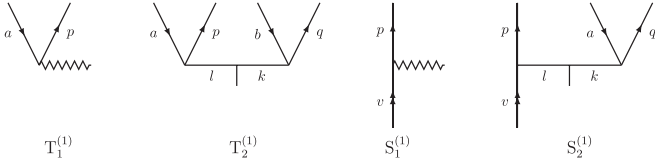
FIG. 1. Diagrammatic representations of $\mathbf{T}_1^{(1)}$, $\mathbf{T}_2^{(1)}$, $\mathbf{S}_1^{(1)}$, and $\mathbf{S}_2^{(1)}$ perturbed cluster operators.

Here $\xi^{...}_{...}$ represents the cluster amplitude for the operator $\mathbf{S}^{(1)}$. The one-body operator $\mathbf{S}_1^{(1)}$ is an odd parity operator and expressed in terms of a rank-one **C**-tensor. It satisfies the orbital-parity and orbital-triangular selection rules, $(-1)^{l_v+l_p} = -1$ and $|j_v - j_p| \leqslant 1 \leqslant (j_v + j_p)$, respectively. The tensor structure of the two-body operator $\mathbf{S}_2^{(1)}$ involves

two **C**-tensors with ranks l and k associated with its two-vertices. These two **C**-tensors are coupled to give a rank-one operator, $\mathbf{S}_2^{(1)}$. The allowed orbital-parity and and orbital-triangular selections rules for $\mathbf{S}_2^{(1)}$ are $(-1)^{l_v+l_p} = -(-1)^{l_a+l_q}$ and $|j_v - j_p| \leqslant l \leqslant (j_v + j_p)$, $|j_a - j_q| \leqslant k \leqslant (j_a + j_q)$, respectively. The diagrammatic representations of $\mathbf{T}^{(1)}$ and $\mathbf{S}^{(1)}$ are shown in Fig. 1.

In analogy with Eq. (2), $|\tilde{\Psi}_v\rangle$ is the solution of the eigenvalue equation

$$(H^{\mathrm{DCB}} + \lambda H_1)|\tilde{\Psi}_v\rangle = \tilde{E}_v|\tilde{\Psi}_v\rangle; \tag{8}$$

here, within the first-order time-independent perturbation theory, the perturbed energy $\tilde{E}_v \equiv E_v$ as the first-order correction vanishes due to the odd parity nature of H_1. Using Eq. (6) in the eigenvalue equation (8) and by operating with $e^{-T^{(0)}}$ from the left, retaining the terms first order in λ, we get

$$[e^{-T^{(0)}}H^{\mathrm{DCB}}e^{T^{(0)}}(\mathbf{S}^{(1)} \cdot \mathbf{E}_{\mathrm{ext}}) + e^{-T^{(0)}}H^{\mathrm{DCB}}e^{T^{(0)}}(\mathbf{T}^{(1)} \cdot \mathbf{E}_{\mathrm{ext}})(1 + S^{(0)}) + e^{-T^{(0)}}H_1e^{T^{(0)}}(1 + S^{(0)})]|\Phi_v\rangle$$
$$= [E_v(\mathbf{S}^{(1)} \cdot \mathbf{E}_{\mathrm{ext}}) + E_v(\mathbf{T}^{(1)} \cdot \mathbf{E}_{\mathrm{ext}})(1 + S^{(0)})]|\Phi_v\rangle. \tag{9}$$

Using the definition of the normal ordered Hamiltonian, $H_N = H^{\mathrm{DCB}} - \langle\Phi_v|H^{\mathrm{DCB}}|\Phi_v\rangle$, and dropping E_{ext} for simplicity from both sides of the equation, we can write

$$[\bar{H}_N\mathbf{S}^{(1)} + \bar{H}_N\mathbf{T}^{(1)}(1 + S^{(0)}) + \bar{H}_1(1 + S^{(0)})]|\Phi_v\rangle$$
$$= \Delta E_v[\mathbf{S}^{(1)} + \mathbf{T}^{(1)}(1 + S^{(0)})]|\Phi_v\rangle, \tag{10}$$

where $\Delta E_v, = E_v - \langle\Phi_v|H^{\mathrm{DCB}}|\Phi_v\rangle$ is the correlation energy of one-valence atom. $\bar{H}_N = e^{-T^{(0)}}H_Ne^{T^{(0)}}$ is a similarity transformed Hamiltonian. Using Wick's theorem, it can be reduced

to

$$\bar{H}_N = H_N + \{\overline{H_N T^{(0)}}\} + \frac{1}{2!}\{\overline{H_N T^{(0)}}T^{(0)}\}$$
$$+ \frac{1}{3!}\{\overline{\overline{H_N T^{(0)}}T^{(0)}}T^{(0)}\} + \frac{1}{4!}\{\overline{\overline{\overline{H_N T^{(0)}}T^{(0)}}T^{(0)}}T^{(0)}\} \tag{11}$$

By projecting Eq. (10) with singly and doubly excited determinants, $\langle\Phi_v^p|$ and $\langle\Phi_{va}^{pq}|$, respectively, and using Wicks's theorem to remove the disconnected terms, we obtain the PRCC coupled equations for singles and doubles as

$$\langle\Phi_v^p|\bar{H}_1 + \{\overline{\bar{H}_1 S^{(0)}}\} + \{\overline{\bar{H}_N \mathbf{T}^{(1)}(1 + S^{(0)})}\} + \{\overline{\bar{H}_N\mathbf{S}^{(1)}}\}\Phi_v\rangle = E_v^{\mathrm{att}}\langle\Phi_v^p|\mathbf{S}_1^{(1)}|\Phi_v\rangle, \tag{12a}$$

$$\langle\Phi_{va}^{pq}|\bar{H}_1 + \{\overline{\bar{H}_1 S^{(0)}}\} + \{\overline{\bar{H}_N \mathbf{T}^{(1)}(1 + S^{(0)})}\} + \{\overline{\bar{H}_N\mathbf{S}^{(1)}}\}\Phi_v\rangle = E_v^{\mathrm{att}}\langle\Phi_{va}^{pq}|\mathbf{S}_2^{(1)}|\Phi_v\rangle. \tag{12b}$$

Here E_v^{att} is the attachment energy of the valence electron and is expressed as $E_v^{\mathrm{att}} = \epsilon_v + \Delta E_v$, where ϵ_v is the single-particle energy. In deriving these equations we have used the relations $\langle\Phi_v^*|\mathbf{T}^{(1)}|\Phi_v\rangle = 0$ and $\langle\Phi_v^*|\mathbf{T}^{(1)}S^{(1)}|\Phi_v\rangle = 0$, as they do not contribute, where $*$ represents the single and doubly excited determinant. We solve these coupled nonlinear equations using the Jacobi method. To remedy the slow convergence of this method we employ direct inversion of the iterated subspace [43].

C. Linearized PRCC

Equations (12a) and (12b) contain all the CC terms associated with the PRCC equations of the one-valence system and therefore provide an accurate description of the properties of the system. However, solving these equations is compu-

tationally expensive due to the large number of many-body diagrams arising from the contractions with multiple CC operators. One simple approach to mitigate this is to retain terms which are linear in the CC operators. This also provides reliable results as in most of the cases the contribution from the nonlinear terms is small. Retaining the terms linear in CC operators, we can write Eqs. (12a) and (12b) as

$$\langle\Phi_v^p|H_1 + \{\overline{H_1 T^{(0)}}\} + \{\overline{H_1 S^{(0)}}\} + \{\overline{H_N \mathbf{T}^{(1)}}\} + \{\overline{H_N\mathbf{S}^{(1)}}\}\Phi_v\rangle$$
$$= E_v^{\mathrm{att}}\langle\Phi_v^p|\mathbf{S}_1^{(1)}|\Phi_v\rangle, \tag{13a}$$

$$\langle\Phi_{va}^{pq}|H_1 + \{\overline{H_1 T^{(0)}}\} + \{\overline{H_1 S^{(0)}}\} + \{\overline{H_N \mathbf{T}^{(1)}}\} + \{\overline{H_N\mathbf{S}^{(1)}}\}\Phi_v\rangle$$
$$= E_v^{\mathrm{att}}\langle\Phi_{va}^{pq}|\mathbf{S}_2^{(1)}|\Phi_v\rangle. \tag{13b}$$

We refer to these equations as the linearized perturbed coupled-cluster (LPRCC) equations. The LPRCC equations
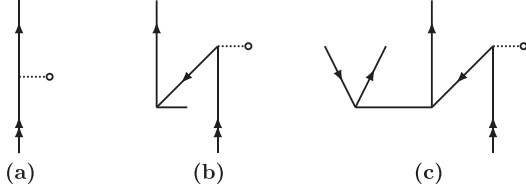
FIG. 2. Single and double PRCC diagrams contributing to the term $\bar{\mathbf{D}}$ of Eqs. (12a) and (12b), respectively.

incorporate all the important many-body effects like random-phase approximation and provide a good description of the one-valence atomic or ionic properties in the presence of perturbation.

D. PRCC diagrams

To solve the coupled-cluster amplitude Eqs.(12a) and (12b), we have to evaluate all the possible terms arising from each of the matrix elements in the equations. There are several terms, and the bookkeeping is simplified with the many-body Goldstone diagrammatic approach. In this section we describe the Goldstone diagrams arising from the matrix elements, and these are evaluated manually. It is, however, possible to identify diagrams computationally as well [44]. We have adopted the manual approach for the convenience in evaluating the angular factors. For simplicity, from here onwards, as should be the case for α, we use $\mathbf{D}$ in place of H_1.

1. $\bar{\mathbf{D}}$

For the one-valence system, from the definition of the similarity transformed Hamiltonian in Eq. (11), using the CCSD approximation we get

$$\bar{\mathbf{D}} = \mathbf{D} + \overline{\mathbf{D}T}_1^{(0)} + \overline{\mathbf{D}T}_2^{(0)}. \tag{14}$$

The terms with two or higher orders of $T^{(0)}$ do not contribute to the PRCC equation for a one-valence system. The first term, $\mathbf{D}$, is the bare dipole operator and contributes to the equation of $\mathbf{S}_1^{(1)}$. The two remaining terms represent the contraction with the unperturbed operator $T^{(0)}$ and contribute to the PRCC equations of the $\mathbf{S}_1^{(1)}$ and $\mathbf{S}_2^{(1)}$, respectively. In total, there are three diagrams from $\bar{\mathbf{D}}$, and these are shown in Fig. 2. Using the algebra of evaluating the Goldstone diagrams [45], we can write the algebraic expressions of the diagrams as

$$\langle \mathbf{D} \rangle_v^p + \langle \overline{\mathbf{D}T}^{(0)} \rangle_v^p = \mathbf{r}_{pv} - \sum_a \mathbf{r}_{av} t_a^p, \tag{15a}$$

$$\langle \overline{\mathbf{D}T}^{(0)} \rangle_{va}^{pq} = -\sum_b \mathbf{r}_{bv} t_{ab}^{qp}, \tag{15b}$$

respectively. Here in atomic units $\mathbf{D} \equiv -\mathbf{r}$ and $\mathbf{r}_{ij} = \langle i|\mathbf{r}|j \rangle$ is the electronic part of the single-particle matrix element of the dipole operator, and $\langle \cdots \rangle_v^p$ and $\langle \cdots \rangle_{vb}^{pq}$ represent the matrix elements $\langle \Phi_v^p | \cdots | \Phi_v \rangle$ and $\langle \Phi_{va}^{pq} | \cdots | \Phi_v \rangle$, respectively.

2. $\bar{\mathbf{D}}S^{(0)}$

Like the first term, consider the second term in Eqs. (12a) and (12b). Expanding the similarity transformed operator $\bar{\mathbf{D}}$ in
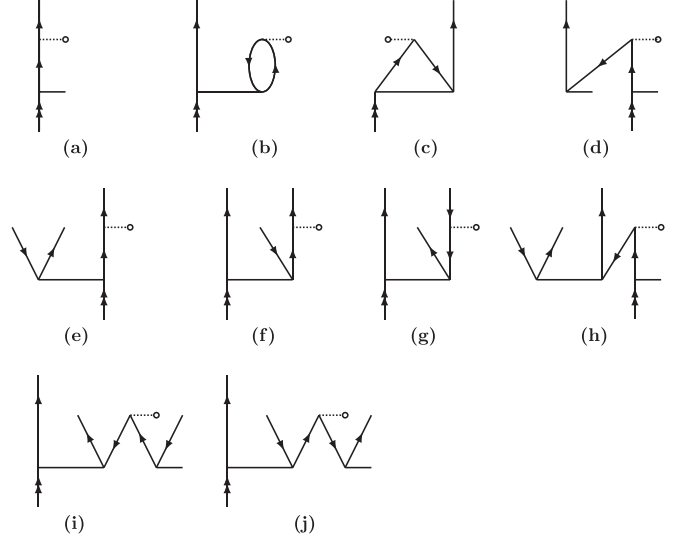

FIG. 3. Single and double PRCC diagrams contributing to the term $\bar{\mathbf{D}}\bar{S}^{(0)}$ of PRCC Eqs. (12a) and (12b), respectively.

terms of $T^{(0)}$, we can write

$$\bar{\mathbf{D}}\bar{S}^{(0)} = \overline{\mathbf{D}S}_1^{(0)} + \overline{\mathbf{D}S}_2^{(0)} + \overline{\mathbf{D}T_1^{(0)}S}_1^{(0)} + \overline{\mathbf{D}T_2^{(0)}S}_1^{(0)}$$
$$+ \overline{\mathbf{D}T_1^{(0)}S}_2^{(0)}. \tag{16}$$

The terms having higher than two orders of CC operators do not contribute. The first three terms in the above equation contribute to the PRCC equation of $\mathbf{S}_1^{(1)}$ and lead to four diagrams. The diagrams are shown in Figs. 3(a)–(d). Except for the first term, all the other terms contribute to the PRCC equation of $\mathbf{S}_2^{(1)}$. In total there are six diagrams from these terms, and these are shown in Figs. 3(e)–(j). The corresponding algebraic expressions are

$$\langle \overline{\mathbf{D}S}^{(0)} \rangle_v^p + \langle \overline{\mathbf{D}T^{(0)}S}^{(0)} \rangle_v^p$$
$$= \sum_q \mathbf{r}_{pq} s_v^q + \sum_{aq} \mathbf{r}_{aq} (s_{va}^{pq} - s_{va}^{qp} - t_a^p s_v^q), \tag{17a}$$

$$\langle \overline{\mathbf{D}S}^{(0)} \rangle_{va}^{pq} + \langle \overline{\mathbf{D}T^{(0)}S}^{(0)} \rangle_{va}^{pq}$$
$$= \sum_r (\mathbf{r}_{pr} s_{av}^{qr} + \mathbf{r}_{qr} s_{va}^{pr}) - \sum_b \mathbf{r}_{ba} s_{vb}^{pq}$$
$$- \sum_{br} \mathbf{r}_{br} (t_{ab}^{qp} s_v^r + t_a^r s_{vb}^{pq} + t_b^q s_{va}^{pr}). \tag{17b}$$

This term is an important one in PRCC theory as it subsumes the many-body effects of the core polarization.

3. $\bar{H}_N \mathbf{T}^{(1)}$

Unlike the previous two terms where the dipole operator appears explicitly, in this term the effects of the perturbation is embedded in a rank one operator, $\mathbf{T}^{(1)}$. We can expand this as

$$\overline{H_N \mathbf{T}}^{(1)} = \overline{H_N \mathbf{T}}^{(1)} + \overline{H_N T^{(0)} \mathbf{T}}^{(1)} + \frac{1}{2} \overline{H_N T^{(0)} T^{(0)} \mathbf{T}}^{(1)}. \tag{18}$$
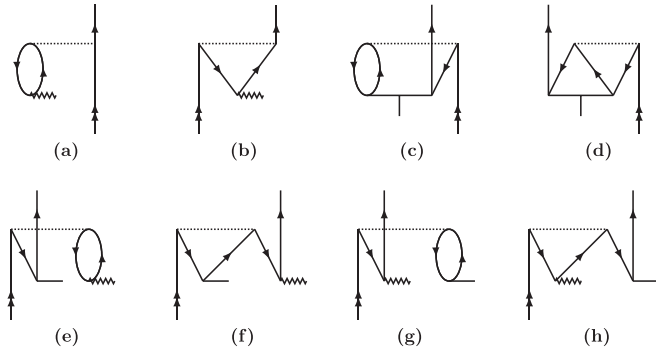
FIG. 4. Single PRCC diagrams contributing to the term $\overline{H_N \mathbf{T}}^{(1)}$ of Eq. (12a).

Consider first the PRCC equation of the $\mathbf{S}_1^{(1)}$. Only the first two terms contribute. The PRCC diagrams from these terms are

obtained by invoking all the possible contractions between the H_N and CC operators. There are eight diagrams, and these are shown in Fig. 4. We do not consider the diagrams arising from the one-body part of H_N. These do not contribute as we use Dirac-Fock orbitals in our calculations. The algebraic expression of these diagrams are given in Eq. (19a). In the equation, g_{ijkl} represents the matrix element $\langle ij|1/r_{12} + g^B(r_{12})|kl\rangle$ and $\tilde{g}_{ijkl}, = (g_{ijkl} - g_{ijlk})$, is an antisymmetric matrix element.

In the PRCC equation of $\mathbf{S}_2^{(1)}$, all the terms contribute and lead to 29 diagrams. These diagrams are shown in Fig. 5. Like in the case of $\mathbf{S}^{(1)}$, we do not include the diagrams from the one-body part of the H_N. The algebraic expression of these diagrams are given in Eq. (19b). In the equation we see the emergence of a trend. The number of terms in this equation far exceed those in $\mathbf{S}_1^{(1)}$. This trend is there in the remaining nonlinear terms as well:

$$\langle \overline{H_N \mathbf{T}}^{(1)}\rangle_v^p + \langle \overline{H_N \overline{T}^{(0)}\mathbf{T}}^{(1)}\rangle_v^p = \sum_{aq} \tilde{g}_{apqv}\tau_a^q + \sum_{abq}\left[-\tilde{g}_{abqv}\tau_{ab}^{qp} + g_{abvq}\left(-t_a^p\tau_b^q + t_a^q\tau_b^p - t_b^q\tau_a^p + t_b^p\tau_a^q\right)\right], \tag{19a}$$

$$\langle \overline{H_N \mathbf{T}}^{(1)}\rangle_{va}^{pq} + \langle \overline{H_N \overline{T}^{(0)}\mathbf{T}}^{(1)}\rangle_{va}^{pq} + \langle \overline{\overline{H_N \overline{T}^{(0)}\overline{T}^{(0)}}\mathbf{T}}^{(1)}\rangle_{va}^{pq} = -\sum_b g_{bqva}\tau_b^p + \sum_{bc}g_{bcva}\tau_{bc}^{pq} - \sum_{br}\left[g_{bpvr}\tau_{ba}^{rq} + g_{bqvr}\left(\tau_{ba}^{pr}\right.\right.$$

$$\left.\left. + \tau_b^p t_a^r + t_b^p\tau_a^r\right)\right] + \sum_{bc}g_{bcva}\left(\tau_b^p t_c^q + t_b^p\tau_c^q\right) + \sum_{bcr}g_{bcvr}\left(-t_{ba}^{pq}\tau_c^r + t_{ab}^{qr}\tau_c^p + t_{ba}^{pr}\tau_c^q + t_{bc}^{pq}\tau_a^r + t_{ca}^{pq}\tau_b^r - t_{ca}^{rq}\tau_b^p + t_{ac}^{rq}\tau_b^p\right.$$

$$\left. - \tau_{ba}^{pq}t_c^r + \tau_{ab}^{qr}t_c^p + \tau_{ba}^{pr}t_c^q + \tau_{bc}^{pq}t_a^r + \tau_{ca}^{pq}t_b^r - \tau_{ca}^{rq}t_b^p + \tau_{ac}^{rq}t_b^p + \tau_a^r t_b^p t_c^q + \tau_c^q t_b^p t_b^q + \tau_b^p t_a^r\right). \tag{19b}$$

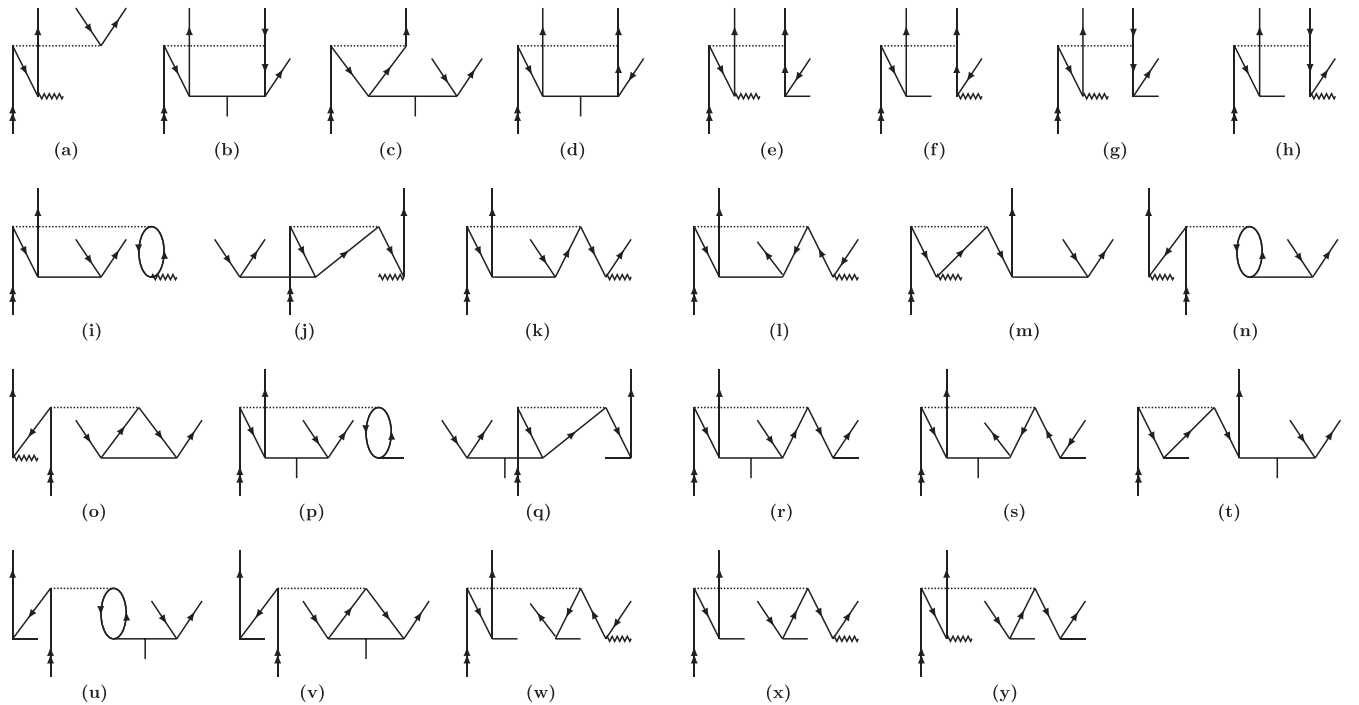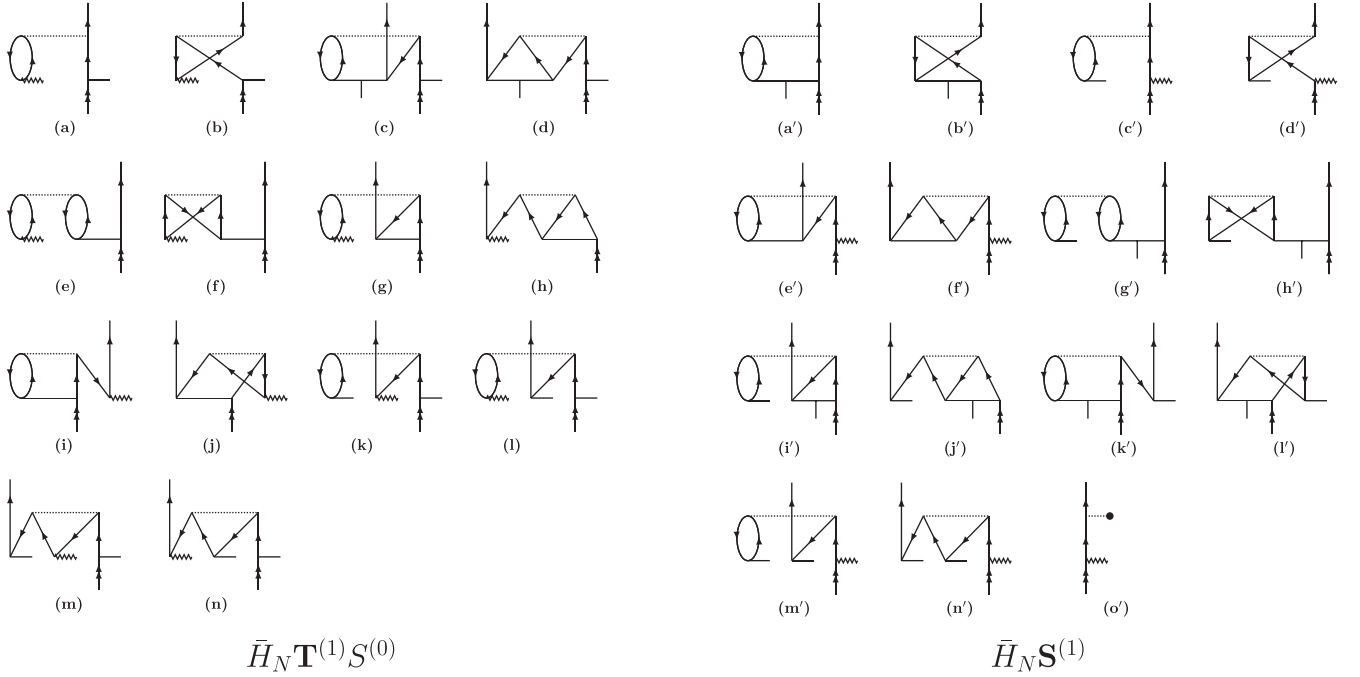FIG. 5. Double PRCC diagrams contributing to the term $\overline{H_N \mathbf{T}}^{(1)}$ of Eq. (12b).

FIG. 6. Single PRCC diagrams contributing to the terms $\overline{\bar{H}_N \mathbf{T}^{(1)} S^{(0)}}$ (a) and $\overline{\bar{H}_N \mathbf{S}^{(1)}}$ (b) of Eq. (12a).

4. $\bar{H}_N \mathbf{T}^{(1)} \mathbf{S}^{(0)}$

This term involves one each of the perturbed and unperturbed CC operators $\mathbf{T}^{(1)}$ and $S^{(0)}$, respectively, and the term contributes to the nonlinear PRCC equation. By expanding $\bar{H}_N$, we obtain

$$\overline{\bar{H}_N \mathbf{T}^{(1)} S^{(0)}} = \overline{H_N \mathbf{T}^{(1)} S^{(0)}} + \overline{H_N T^{(0)} \mathbf{T}^{(1)} S^{(0)}}. \tag{20}$$

The higher order terms will not contribute. As to be expected, several diagrams arise from this term due to various possible contractions between H_N and CC operators. For the PRCC equation of $\mathbf{S}_1^{(1)}$, there are 14 diagrams from this term, and these are are shown in the left panel of Fig. 6. The algebraic expressions of these diagrams are given in Eq. (21):

$$\langle \overline{H_N \mathbf{T}^{(1)} S^{(0)}} \rangle_v^p + \langle \overline{H_N T^{(0)} \mathbf{T}^{(1)} S^{(0)}} \rangle_v^p = \sum_{aqr} g_{apqr}\left(\tau_a^q s_v^r - \tau_a^r s_v^q\right) + \sum_{aqbr} g_{abqr}\left[s_v^r\left(-\tau_{ab}^{qp} + \tau_{ab}^{pq}\right) + \tau_a^q s_{bv}^{rp} + \tau_b^q s_{av}^{rp} - \tau_a^q s_{bv}^{pr} \right.$$

$$\left. + \tau_a^p s_{bv}^{qr} - \tau_b^p s_{av}^{qr} + \tau_b^q s_{av}^{pr} + \left(-\tau_b^p t_a^q - \tau_a^q t_b^p + \tau_b^q t_a^p + \tau_a^p t_b^q\right)s_v^r \right], \tag{21}$$

$$\langle \overline{H_N \mathbf{T}^{(1)} S^{(0)}} \rangle_{va}^{pq} + \langle \overline{H_N T^{(0)} \mathbf{T}^{(1)} S^{(0)}} \rangle_{va}^{pq} = \sum_{rs} g_{pqrs}\tau_a^s s_v^r - \sum_{rb}\left(g_{pbra}\tau_b^q + g_{qbar}\tau_b^p\right)s_v^r + \sum_{sbr} g_{pbsr}\left[s_v^s(\tau_{ba}^{rq} - \tau_{ab}^{rq}) - s_v^r(\tau_{ab}^{qs} + \tau_{ab}^{sp})\right]$$

$$+ \sum_{cbr} g_{cbar}\tau_{cb}^{qp}s_v^r + \sum_{brs} g_{bprs}(s_{va}^{sq}\tau_b^r - s_{va}^{rq}\tau_b^s - s_{bv}^{qs}\tau_a^r - s_{av}^{rs}\tau_b^q - s_{bv}^{pr}\tau_a^s - s_{bv}^{sp}\tau_a^r + s_{sp}^{av}\tau_b^r$$

$$- s_{rs}^{va}\tau_b^p + s_{bv}^{rp}\tau_a^s - s_{av}^{rp}\tau_b^s) + \sum_{cbr} g_{cbar}\left[s_{bv}^{pr}\tau_c^q - s_{cv}^{qp}\tau_b^r + s_{cv}^{rp}\tau_b^q + s_{bv}^{qp}\tau_c^r - s_{bv}^{rp}\tau_c^q + s_{vc}^{rq}\tau_b^p\right]$$

$$+ \sum_{bcrs} g_{bcrs}\left[s_{cv}^{sp}\tau_{ab}^{qr} + s_{cv}^{rp}\tau_{ab}^{qs} - s_{cv}^{sp}\tau_{ab}^{rq} + s_{cv}^{qp}\tau_{ab}^{rs} + s_{av}^{sp}\tau_{bc}^{qr} - s_{cv}^{ps}\tau_{ab}^{qr} + s_{cv}^{rs}\tau_{ab}^{qp}\right.$$

$$\left. + s_{vc}^{rp}\tau_{ab}^{qs} + s_{vc}^{sp}\tau_{ab}^{rq} - s_{vc}^{rs}\tau_{ab}^{qp} - s_{av}^{sp}\tau_{bc}^{rq} - s_{cv}^{qp}\tau_{ba}^{rs}\right], \tag{22}$$
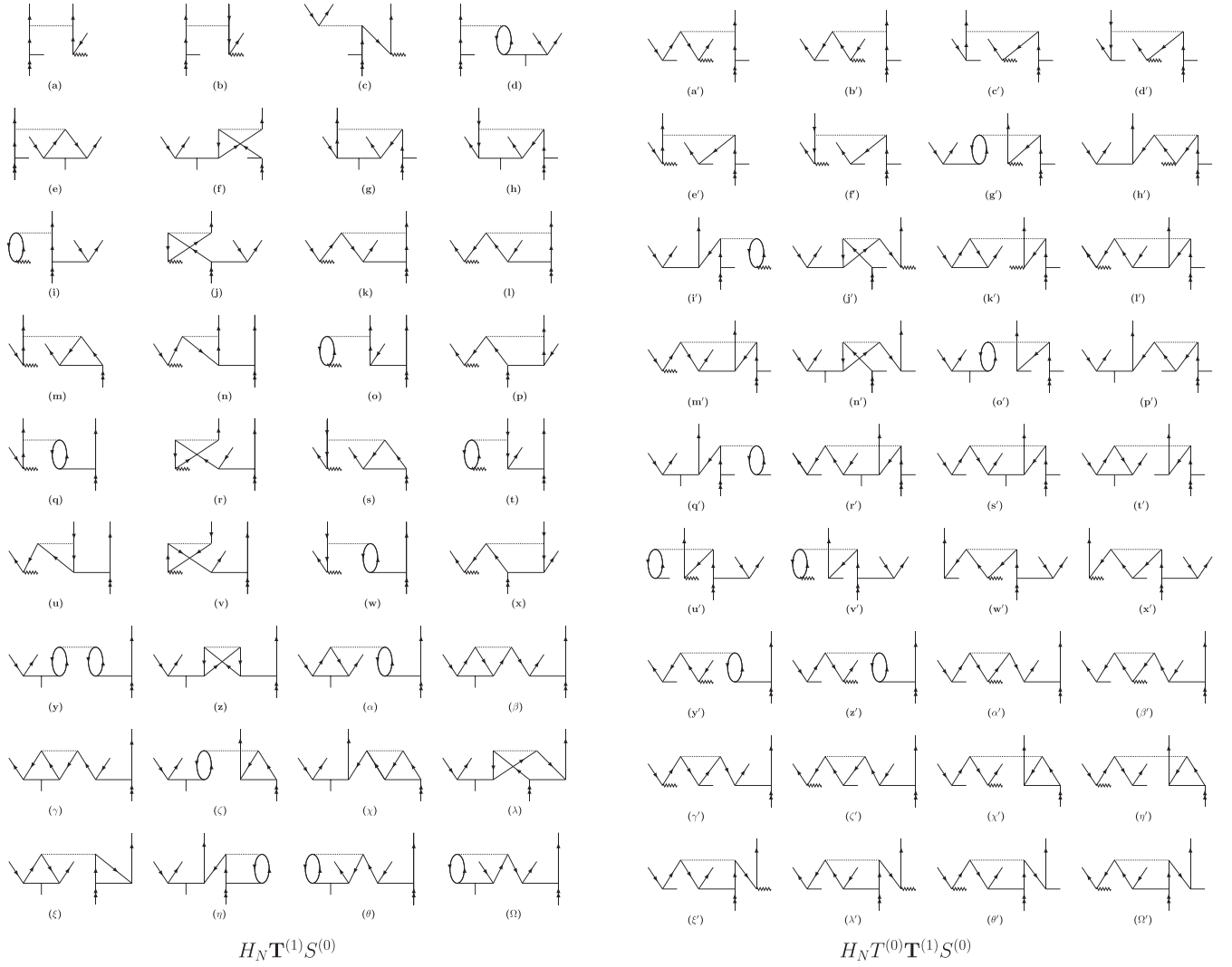
FIG. 7. Double PRCC diagrams contributing to the terms $\overline{H_N \mathbf{T}^{(1)} S^{(0)}}$ (left panel) and $\overline{H_N T^{(0)} \mathbf{T}^{(1)} S^{(0)}}$ (right panel) of Eq. (12b).

$$
\left\langle \overline{H_N \overline{T^{(0)}} \mathbf{T}^{(1)} S^{(0)}} \right\rangle^{pq}_{va} + \left\langle \overline{H_N \overline{T^{(0)}} \mathbf{T}^{(1)} S^{(0)}} \right\rangle^{pq}_{va} = \sum_{brs} g_{bprs} \left[\left(-t^r_a \tau^q_b - t^q_b \tau^r_a \right) s^s_v - \left(t^s_a \tau^p_b + t^p_b \tau^s_a \right) s^r_v \right] + \sum_{brc} g_{bcar} \left(t^q_b \tau^p_c + t^p_c \tau^q_b \right) s^r_v
$$

$$
+ \sum_{brcs} g_{bcrs} \left[\left(-t^{qr}_{ab} \tau^p_c + t^{qp}_{ab} \tau^r_c \right) s^s_v + \left(-t^{qp}_{ab} \tau^s_c + t^{qs}_{ab} \tau^p_c \right) s^r_v + \left(t^{rq}_{ab} \tau^p_c + t^{rp}_{ac} \tau^q_b + t^{qp}_{bc} \tau^r_a \right) s^s_v \right.
$$

$$
+ \left(\tau^{qs}_{ab} t^p_c - \tau^{qr}_{ab} t^p_c + \tau^{qp}_{ab} t^r_c - \tau^{qp}_{ac} t^r_b + \tau^{rp}_{ac} t^q_b + \tau^{qp}_{bc} t^r_a + \tau^{rq}_{ab} t^p_c \right) s^s_v
$$

$$
+ \left[-t^r_b \tau^p_c - t^p_c \tau^r_b + t^p_b \tau^r_c + \tau^p_b t^r_c \right] s^{sq}_{va} + \left(-t^q_b \tau^r_a - \tau^q_b t^r_a \right) s^{sp}_{cv} + \left(t^r_c \tau^q_b + \tau^r_c t^q_b \right) s^{sp}_{av}
$$

$$
+ \left(t^s_b \tau^r_a + \tau^s_b t^r_a \right) s^{qp}_{cv} + \left(t^r_a \tau^q_b + \tau^r_a t^q_b \right) s^{ps}_{cv} + \left(t^r_a \tau^p_c + \tau^r_a t^p_c \right) s^{qs}_{bv} + \left(t^q_b \tau^p_c + \tau^q_b t^p_c \right) s^{rs}_{av} \right]. \quad (23)
$$

In the case of the PRCC equation for $\mathbf{S}_2^{(1)}$, 72 Goldstone diagrams arise from this term. Out of these, 36 diagrams each arise from the first and second terms. These diagrams are shown in the left and right panels, respectively, of Fig. 7. The algebraic expression of the diagrams in the left panel is given in Eq. (22). Similarly, the algebraic expression of the diagrams in the right panel is given in Eq. (23).
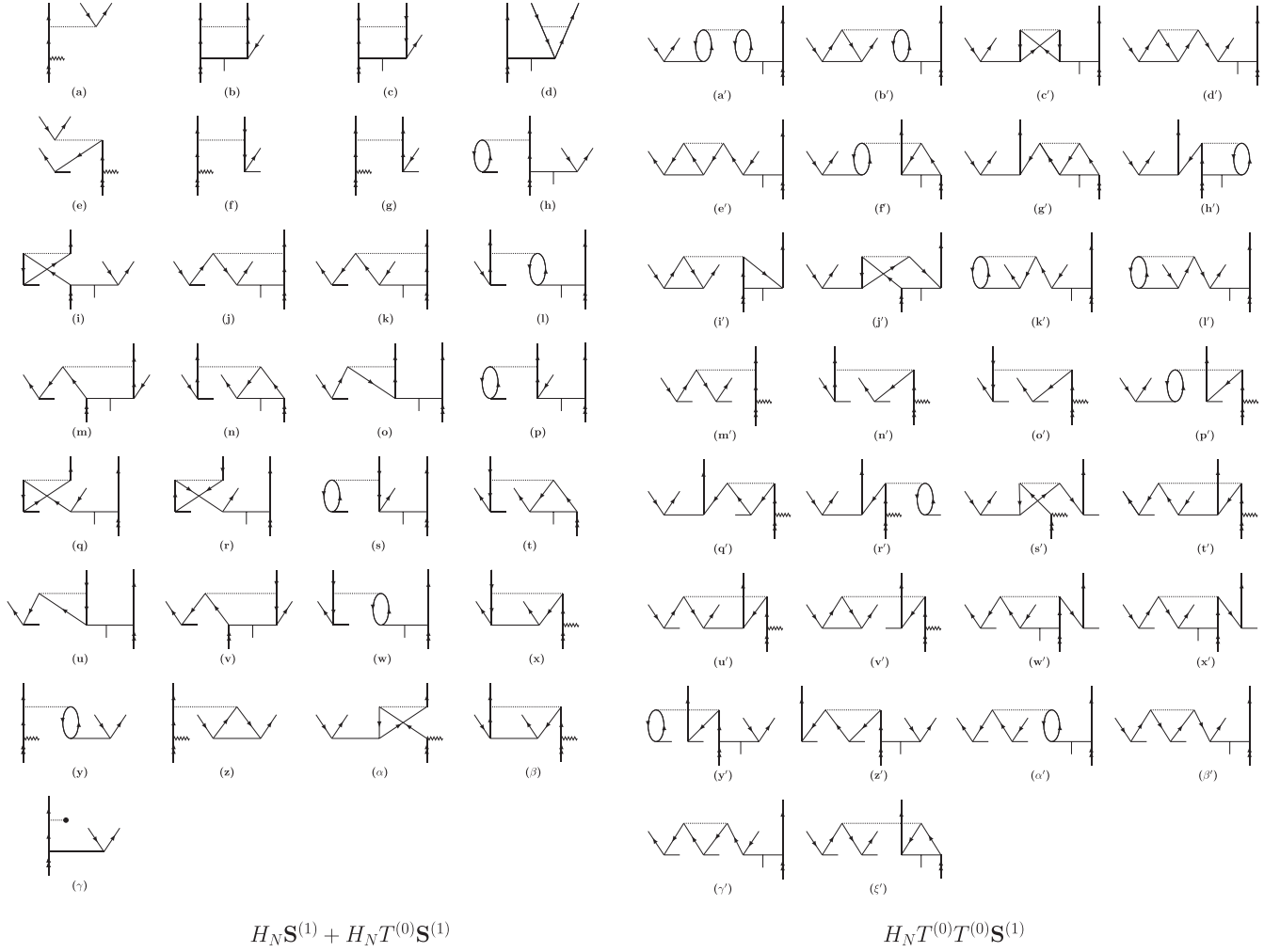
FIG. 8. Double PRCC diagrams contributing to the terms $\overline{H_N \mathbf{S}}^{(1)} + \overline{H_N T^{(0)} \mathbf{S}}^{(1)}$ (left panel) and $\overline{H_N T^{(0)} T^{(0)} \mathbf{S}}^{(1)}$ (right panel) of Eq. (12b).

5. $\bar{H}_N \mathbf{S}^{(1)}$

This term contains a perturbed operator, $\mathbf{S}^{(1)}$, which subsumes dominant effects of perturbation for one-valence atomic systems. Expanding $\bar{H}_N$

$$\overline{\bar{H}_N \mathbf{S}}^{(1)} = \overline{H_N \mathbf{S}}^{(1)} + \overline{H_N T^{(0)} \mathbf{S}}^{(1)} + \frac{1}{2!} \overline{H_N T^{(0)} T^{(0)} \mathbf{S}}^{(1)}. \tag{24}$$

In the PRCC equation of $\mathbf{S}_1^{(1)}$, both the one- and two-body CC operators from the first and second terms contribute. From the third term, however, only the term $H_N T_1^{(0)} T_1^{(0)} S_1^{(1)}$ contributes. There are 15 diagrams that contribute to the PRCC equation of $\mathbf{S}_1^{(1)}$, and these are shown in the right panel of Fig. 6. The algebraic expression of these diagrams is given in Eq. (25).

For the PRCC equation of $\mathbf{S}_2^{(1)}$, there are in total 59 diagrams. Out of these 29 diagrams arise from the first two terms. These diagrams are shown in the left panel of Fig. 8. The remaining 30 diagrams arise from the third term and are shown in the right panel of Fig. 8. The algebraic expression of diagrams in the left and right panels is given in Eqs. (26) and (27), respectively:

$$\langle \overline{H_N \mathbf{S}}^{(1)} \rangle_v^p + \langle \overline{H_N T^{(0)} \mathbf{S}}^{(1)} \rangle_v^p + \overline{H_N T^{(0)} T^{(0)} \mathbf{S}}^{(1)} \rangle_v^p = \sum_{aqr} g_{apqr} \left(\xi_{av}^{qr} - \xi_{av}^{rq} + t_a^q \xi_v^r - t_a^r \xi_v^q \right) + \sum_{aqbr} g_{abqr} \Big[\left(-t_{ab}^{qp} + t_{ab}^{pq} \right) \xi_v^r + t_a^q \xi_{bv}^{rp}$$

$$+ t_b^q \xi_{av}^{rp} - t_a^q \xi_{bv}^{pr} + t_a^p \xi_{bv}^{qr} - t_b^p \xi_{av}^{qr} + t_b^q \xi_{av}^{pr} + \frac{1}{2!} \left(-t_a^q t_b^p + t_a^p t_b^q \right) \xi_v^r + \sum_q g_q^p \xi_v^q, \tag{25}$$

$$\langle \overline{H_N \mathbf{S}}^{(1)}\rangle_{va}^{pq} + \langle \overline{H_N T^{(0)}\mathbf{S}}^{(1)}\rangle_{va}^{pq} = \sum_r g_{pqra}\xi_v^r + \sum_{rs} g_{pqrs}\xi_{va}^{rs} - \sum_{rb}(g_{pbra}\xi_{vb}^{rq} + g_{bqar}\xi_{vb}^{pr}) + \sum_{br}\left[-t_b^p g_{qbar} - t_b^q g_{pbra}\right]\xi_v^r$$

$$+ \sum_{rs} g_{pqrs}t_a^s\xi_v^r + \sum_{bsr}\left[g_{bpsr}(t_b^s\xi_{va}^{rq} - t_b^r\xi_{va}^{sq} - t_a^s\xi_{bv}^{qr} - t_b^q\xi_{av}^{sr}) + g_{bqsr}(t_a^r\xi_{bv}^{sp} - t_b^p\xi_{va}^{sr} - t_a^r\xi_{bv}^{ps}\right.$$

$$\left.-t_a^s\xi_{bv}^{rp} + t_b^s\xi_{av}^{rp} - t_b^r\xi_{av}^{sp})\right] + \sum_{rbc} g_{bcra}\left[t_c^r\xi_{bv}^{qp} - t_b^r\xi_{cv}^{qp} + t_c^q\xi_{bv}^{pr} + t_b^q\xi_{cv}^{rp} + t_b^p\xi_{vc}^{rq} - t_c^q\xi_{bv}^{rp} + t_{cb}^{qp}\xi_v^r\right]$$

$$+ g_{pbsr}\left[(t_{ba}^{rq} - t_{ab}^{rq})\xi_v^s - t_{ab}^{qs}\xi_v^r\right] - g_{qbsr}t_{ab}^{sp})\xi_v^r\right] + \sum_r g_{pr}t_{va}^{rq}, \tag{26}$$

$$\langle \overline{\overline{H_N T^{(0)}T^{(0)}\mathbf{S}}}^{(1)}\rangle_{va}^{pq} = \sum_{brcs} g_{bcrs}\left[(t_{ab}^{qr} - t_{ab}^{rq})\xi_{cv}^{sp} + t_{ab}^{qs}\xi_{cv}^{rp} + t_{ab}^{rs}\xi_{cv}^{qp} + t_{bc}^{qr}\xi_{av}^{sp} - t_{ab}^{qr}\xi_{cv}^{ps} + t_{ab}^{qp}(\xi_{cv}^{rs} - \xi_{vc}^{rs}) + t_{ab}^{rq}\xi_{vc}^{sp}\right.$$

$$+ t_{ab}^{qs}\xi_{vc}^{rp} - t_{bc}^{rq}\xi_{av}^{sp} - t_{ba}^{rs}\xi_{cv}^{qp}\right] + \sum_{rbs}\left[-g_{bprs}t_a^r t_b^q\xi_v^s - g_{bqrs}t_a^s t_b^p\xi_v^r\right] + \sum_{cbr} g_{cbar}t_c^q t_b^p\xi_v^r + \sum_{brcs} g_{bcrs}\left[\left(-t_{ab}^{qr}t_c^p\right.\right.$$

$$+ t_{ab}^{qp}t_c^r)\xi_v^s + \left(-t_{ab}^{qp}t_c^s + t_{ab}^{qs}t_c^p\right)\xi_v^r + \left(t_{ac}^{rp}t_b^q + t_{bc}^{qp}t_a^r + t_{ab}^{rq}t_c^p\right)\xi_v^s + \left(t_b^q\xi_{av}^{rs} + t_a^r\xi_{bv}^{qs} - t_b^r\xi_{va}^{sq}\right)t_c^p + t_b^p\xi_{va}^{sq}t_c^r$$

$$+ t_a^r\left(-t_b^q\xi_{cv}^{sp} + t_b^s\xi_{cv}^{qp}\right) + t_b^q\left(t_c^r\xi_{av}^{sp} + t_a^r\xi_{cv}^{ps}\right). \tag{27}$$

6. Folded diagrams

The terms on the right-hand sides of the PRCC Eqs. (12a) and (12b) are referred to as the renormalization terms in the CC equation of the one-valence systems. It is an important term, and its nonzero value distinguishes the PRCC equations of open-shell systems from the closed-shell systems. These contribute through the folded diagrams arising from the contraction of the energy with the CC operators. This contraction is not possible in the case of closed-shell systems as the energy diagrams do not have free lines. Folded diagrams contributing to Eqs. (12a) and (12b) are given in Figs. 9(a) and 9(b).

III. POLARIZABILITY FOR ONE-VALENCE USING PRCC

There are three key points for choosing PRCC to compute polarizability over the finite-field approach. First, this is computationally efficient. In this method the coupled-cluster equations are solved only once. However, in the finite-field (FF) approach, CC equations need to be solved at least twice—at two different perturbation strengths—which require more computational time. Second, once implemented, the other properties such as magnetic and hyperfine can be computed with minor change in the implementation to replace the dipole operator. The FF approach, however, is more suitable for the calculation of the electric properties. For other properties, however, its implementation is not that straightforward. And, third, in terms of accuracy, it is equivalent to the FF approach when used with accurate wave functions. A

detailed comparison in terms of implementation, efficiency, and accuracy between these two approaches can be found in Refs. [46,47].

In the PRCC, the electric dipole polarizability α of an atom or ion is defined as the expectation of the dipole operator with respect to the perturbed state $|\tilde{\Psi}_v\rangle$. For the one-valence atomic system

$$\alpha = -\frac{\langle \tilde{\Psi}_v|\mathbf{D}|\tilde{\Psi}_v\rangle}{\langle \Psi_v|\Psi_v\rangle}. \tag{28}$$

Using the expression of $|\tilde{\Psi}_v\rangle$ from Eq. (6) and retaining only the terms with first order in λ, we get

$$\alpha = \frac{1}{\mathcal{N}}\langle \Phi_v|\bar{\mathbf{D}}(\mathbf{S}^{(1)} + \mathbf{T}^{(1)} + \mathbf{T}^{(1)}S^{(0)}) + (\mathbf{S}^{(1)} + \mathbf{T}^{(1)}$$

$$+ \mathbf{T}^{(1)}S^{(0)})^\dagger\bar{\mathbf{D}} + S^{(0)\dagger}\bar{\mathbf{D}}(\mathbf{S}^{(1)} + \mathbf{T}^{(1)} + \mathbf{T}^{(1)}S^{(0)})$$

$$+ (\mathbf{S}^{(1)} + \mathbf{T}^{(1)} + \mathbf{T}^{(1)}S^{(0)})^\dagger\bar{\mathbf{D}}S^{(0)}|\Phi_v\rangle, \tag{29}$$

where

$$\mathcal{N} = \langle \Phi_v|[e^{T^{(0)}}(1 + S^{(0)})]^\dagger[e^{T^{(0)}}(1 + S^{(0)})]|\Phi_v\rangle, \tag{30}$$

is the normalization factor of the eigenstate $|\Psi_v\rangle$ and $\bar{\mathbf{D}}, = e^{T^{(0)\dagger}}\mathbf{D}e^{T^{(0)}}$, is a dressed operator, which is a nonterminating series of the cluster operator $T^{(0)}$. In the present work, however, we consider up to the second-order term $\bar{\mathbf{D}} = \mathbf{D} + \mathbf{D}T^{(0)} + T^{(0)\dagger}\mathbf{D} + T^{(0)\dagger}\mathbf{D}T^{(0)}$. The higher order terms in $T^{(0)}$ have negligible contributions, and this has been confirmed through detailed computations [41]. In the CCSD approximation, Eq. (29) can be written as

$$\alpha = \frac{1}{\mathcal{N}}\langle \Phi_v|\left(\mathbf{DS}_1^{(1)} + \mathbf{DS}_2^{(1)} + S_1^{(0)\dagger}\mathbf{DS}_1^{(1)} + S_1^{(0)\dagger}\mathbf{DS}_2^{(1)} + S_2^{(0)\dagger}\mathbf{DS}_1^{(1)} + S_2^{(0)\dagger}\mathbf{DS}_2^{(1)} + S_1^{(0)\dagger}\mathbf{DT}_1^{(1)} + S_2^{(0)\dagger}\mathbf{DT}_1^{(1)}\right.$$

$$+ S_2^{(0)\dagger}\mathbf{DT}_2^{(1)} + T_1^{(0)\dagger}\mathbf{DS}_1^{(1)} + T_1^{(0)\dagger}\mathbf{DS}_2^{(1)} + T_2^{(0)\dagger}\mathbf{DS}_2^{(1)} + \mathbf{DT}^{(1)} + T_1^{(0)\dagger}\mathbf{DT}_1^{(1)} + T_1^{(0)\dagger}\mathbf{DT}_2^{(1)} + T_2^{(0)\dagger}\mathbf{DT}_1^{(1)}$$

$$\left.+ T_2^{(0)\dagger}\mathbf{DT}_2^{(1)}\right) + \text{H.c} + \mathbf{DT}_1^{(1)}S_1^{(0)} + \mathbf{DT}_1^{(0)}S_1^{(1)}|\Phi_v\rangle. \tag{31}$$
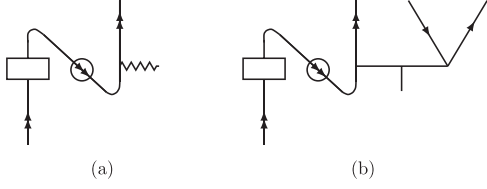
FIG. 9. Folded diagrams contributing to PRCC Eqs. ([12a]) (a) and ([12b]) (b).

Here the terms $S_1^{(0)\dagger}\mathbf{DT}_2^{(1)} + \text{H.c.}$, $T_2^{(0)\dagger}\mathbf{DS}_2^{(1)} + \text{H.c.}$, and $\mathbf{DT}_2^{(1)} + \text{H.c.}$ are not included as these do not contribute to the α of the one-valence system.

A. Diagrams for α

There are 128 Goldstone diagrams which contribute to Eq. ([31]). As an example of the diagrams, in Fig. [10] we show one diagram from each of the terms in Eq. ([31]). The diagrams from the Hermitian conjugate (H.c.) terms are, however, not shown as these are topologically equivalent. Among all the terms in Eq. ([31]), the first four terms, $\mathbf{DS}_1^{(1)}$, $\mathbf{DS}_2^{(1)}$, and their
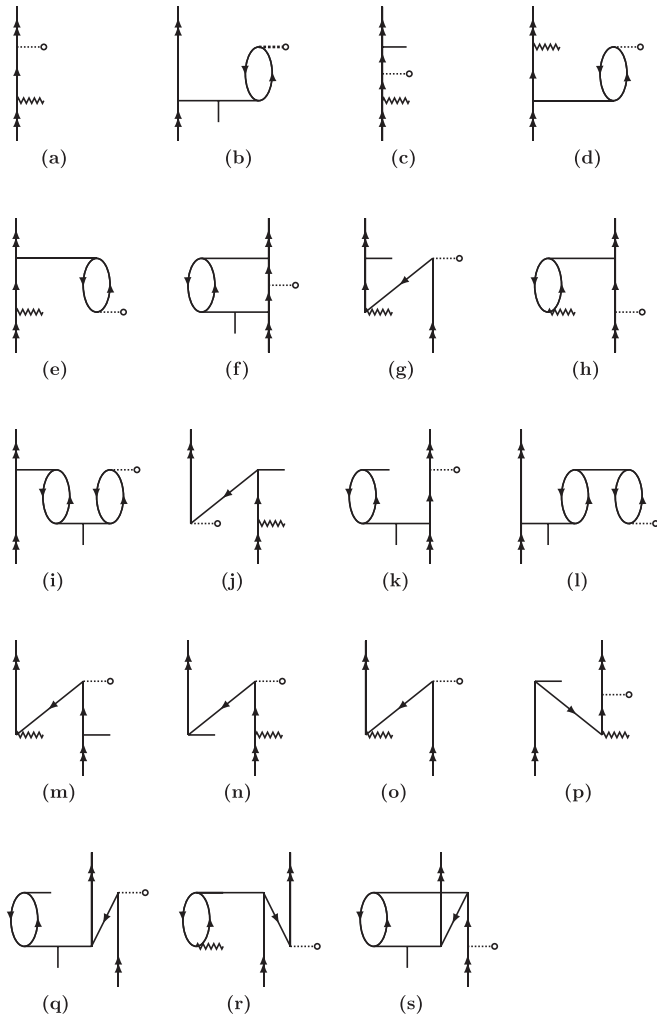

FIG. 10. Some example polarizability diagrams for one-valence atomic system, contributing to Eq. ([31])
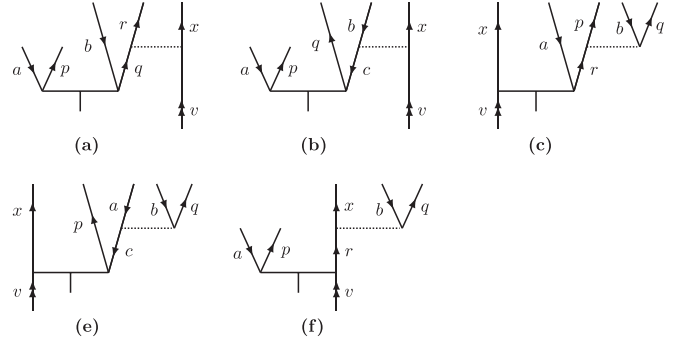

FIG. 11. Perturbative $\mathbf{S}_3^{(1)}$ diagrams arising from $g\overline{\mathbf{T}}_2^{(1)}$ and $g\overline{\mathbf{S}}_2^{(1)}$ contractions. Panels (a), (c), and (f) correspond to the *particle-particle* (p-p), whereas panels (b) and (e) correspond to the *hole-hole* (h-h) type of contractions.

H.c., are expected to have the dominant contribution. The reason for this is the large magnitude of the one-valence cluster operators and the strong effect of the perturbation on these operators. More importantly, the terms $\mathbf{DS}_1^{(1)} + \text{H.c.}$ subsume the contributions from the Dirac-Fock (DF) and the random-phase-approximation (RPA). The diagrams of the $\mathbf{DS}_1^{(1)}$ and $\mathbf{DS}_2^{(1)}$ are shown in Figs. [10(a)] and [10(b)], respectively.

Among the terms with two orders of CC operators, $S_1^{(0)\dagger}\mathbf{DS}_1^{(1)}$, $S_1^{(0)\dagger}\mathbf{DS}_2^{(1)}$, $S_2^{(0)\dagger}\mathbf{DS}_1^{(1)}$, $S_2^{(0)\dagger}\mathbf{DS}_2^{(1)}$, and their H.c., are expected to give dominant contributions. The example diagrams of these four terms are shown in Figs. [10(c)]–[(f)]. The next important contributions are expected from the terms with one each of the T and S operators: $S_1^{(0)\dagger}\mathbf{DT}_1^{(1)}$, $S_2^{(0)\dagger}\mathbf{DT}_1^{(1)}$, $S_2^{(0)\dagger}\mathbf{DT}_2^{(1)}$, $T_1^{(0)\dagger}\mathbf{DS}_1^{(1)}$, $T_1^{(0)\dagger}\mathbf{DS}_2^{(1)}$, $T_2^{(0)\dagger}\mathbf{DS}_2^{(1)}$ and their H.c. and $\mathbf{DT}_1^{(1)}S_1^{(0)}$ and $\mathbf{D}T_1^{(0)}\mathbf{S}_1^{(1)}$. The representative diagrams from these terms are shown in Figs. [10(g)]–[(n)]. The remaining terms, $\mathbf{DT}_1^{(1)}$, $T_1^{(0)\dagger}\mathbf{DT}_1^{(1)}$, $T_1^{(0)\dagger}\mathbf{DT}_2^{(1)}$, $T_2^{(0)\dagger}\mathbf{DT}_1^{(1)}$, $T_2^{(0)\dagger}\mathbf{DT}_2^{(1)}$ and their H.c., having two orders of closed-shell operator, are expected to have the lowest contribution to α. This is due to the small magnitudes of these operators for the open-shell systems. Some representative diagrams from these are shown in Figs. [10(o)]–[(s)].

B. Perturbative triples

To account for the corrections from the triple excitations in PRCC we resort to perturbative triples. The perturbative triples encapsulate dominant contributions from triples, however, at a much lower computational cost than full triples. Since the effect of external perturbation is incorporated through the perturbed operators in PRCC, for this we choose perturbative triples arising from $\mathbf{T}^{(1)}$ and $\mathbf{S}^{(1)}$. At the level of triples, only two-body operators contribute, and these lead to 5 $\mathbf{S}_3^{(1)}$ diagrams (shown in Fig. [11]) after the contractions $g\overline{\mathbf{T}}_2^{(1)}$ and $g\overline{\mathbf{S}}_2^{(1)}$. Here $g_{ij} = \sum_{i<j}[\frac{1}{r_{ij}} + g^B(r_{ij})]$ is the two-body residual interaction. The algebraic expressions for these diagrams (in the sequence of Fig. [11]) are

$$\mathbf{S}_3^{(1)} \approx \frac{a_p^\dagger a_r^\dagger a_x^\dagger a_v a_b a_a}{\Delta\epsilon_{abv}^{prx}} \sum_r \langle rx|g|qv\rangle\langle pq|\mathbf{T}_2^{(1)}|ab\rangle, \quad (32a)$$
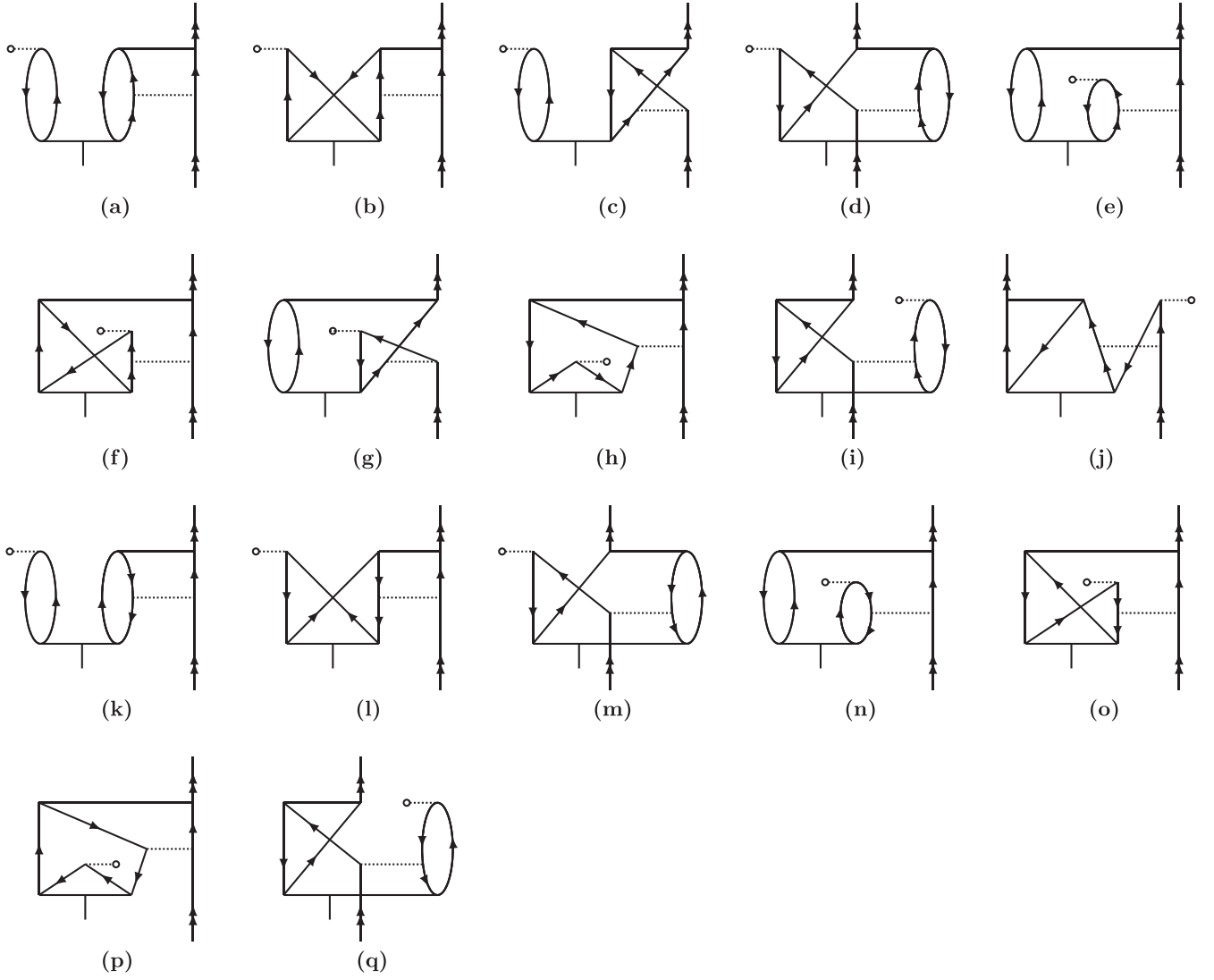
FIG. 12. Polarizability diagrams contributing to the term $S_2^{(0)\dagger}\mathbf{D}g\mathbf{T}_2^{(1)}$.

$$\mathbf{S}_3^{(1)} \approx \frac{a_p^\dagger a_q^\dagger a_x^\dagger a_v a_b a_a}{\Delta\epsilon_{abv}^{pqx}} \sum_c \langle cx|g|bv\rangle\langle pq|\mathbf{T}_2^{(1)}|ac\rangle, \quad (32b)$$

$$\mathbf{S}_3^{(1)} \approx \frac{a_x^\dagger a_p^\dagger a_q^\dagger a_b a_a a_v}{\Delta\epsilon_{vab}^{xpq}} \sum_r \langle pq|g|rb\rangle\langle xr|\mathbf{S}_2^{(1)}|va\rangle, \quad (32c)$$

$$\mathbf{S}_3^{(1)} \approx \frac{a_x^\dagger a_p^\dagger a_q^\dagger a_b a_a a_v}{\Delta\epsilon_{vab}^{xpq}} \sum_c \langle cq|g|ab\rangle\langle xp|\mathbf{S}_2^{(1)}|vc\rangle, \quad (32d)$$

$$\mathbf{S}_3^{(1)} \approx \frac{a_p^\dagger a_x^\dagger a_q^\dagger a_b a_v a_a}{\Delta\epsilon_{vab}^{xpq}} \sum_r \langle xq|g|rb\rangle\langle pr|\mathbf{S}_2^{(1)}|av\rangle, \quad (32e)$$

where $\Delta\epsilon_{abc}^{ijk} = \epsilon_a + \epsilon_b + \epsilon_c - \epsilon_i - \epsilon_j - \epsilon_k$. For the dipole polarizability, the dominant contribution is expected from the contraction of $\mathbf{S}_3^{(1)}$ with the unperturbed operator $S_2^{(0)}$ and the dipole operator. This is due to the larger amplitudes of the $S^{(0)}$ operators for the one-valence systems. There are in total 17 diagrams from the term $S_2^{(0)\dagger}\mathbf{D}g\mathbf{T}_2^{(1)}$. These diagrams are shown in Fig. 12. Similarly, the

term $S_2^{(0)\dagger}\mathbf{D}g\mathbf{S}_2^{(1)}$ has 32 diagrams, and these are given in Fig. 13.

IV. BASIS SET CONVERGENCE

A basis set which provides a good description of the single-electron wave functions and energies is essential to obtain accurate and reliable results using the PRCC theory. Some of the basis sets used in atomic theory calculations are B-spline [48], finite discrete spectrum [49], Slater-type orbitals [50], r multiplied basis [51], and analytical Gaussian basis proposed and optimized by Dyall [52] and Huzinaga [53]. The present implementation of our RCC codes is using the numerical Gaussian-type orbitals (GTOs) [54]. The advantage of the numerical basis is the simplicity of extending the PRCC method to compute other atomic properties like the parity noncon-servation, intrinsic electric dipole moment, QED effects, etc. The use of analytic basis sets in some of these would require additional developments and approximations. Our previous works have shown that the even-tempered GTOs converge faster and predict reliable values of dipole polarizabilities and
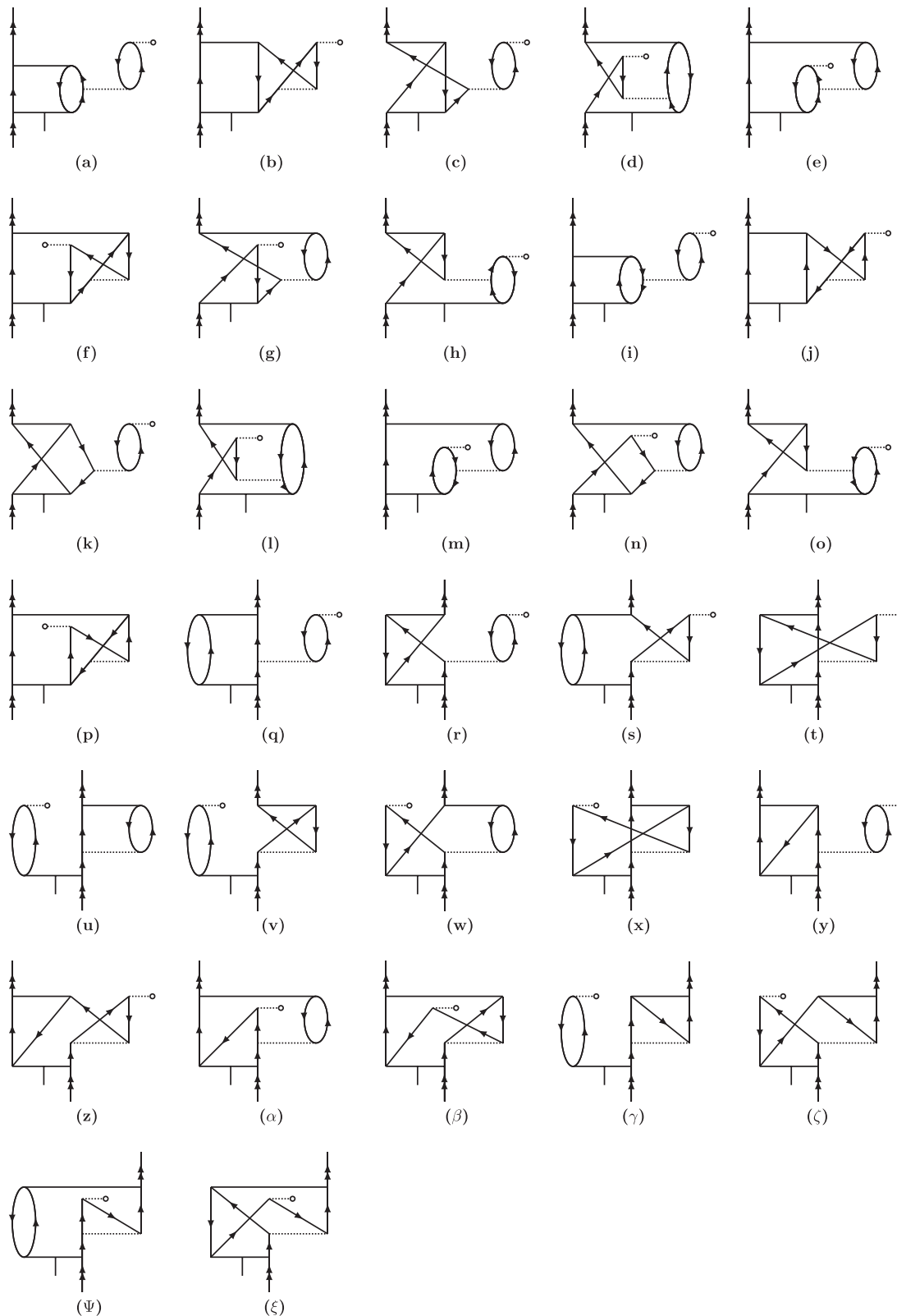
FIG. 13. Polarizability diagrams contributing to the term $S_2^{(0)\dagger} \mathbf{D}_g S_2^{(1)}$.

other atomic properties. Considering this, in the present work, we used even-tempered GTOs [38] as the single-electron basis set. However, to ensure the accuracy of GTOs used in our calculations, the basis parameters are optimized to match the orbital energies as well as the self-consistent field

energies with the GRASP2K [55] results. We achieved an excellent agreement between the GTO and GRASP2K energies. A detailed analysis and comparison of the energies of the group-13 elements is reported in our recent work [31]. To improve the quality of the basis set further, we incorporate

TABLE I. Convergence trend of α (a.u.) and electron correlation energy (cm^{-1}) for ground state with basis size. The values listed are calculated using the Dirac-Coulomb Hamiltonian.

Basis	Orbitals Al	α $^2P_{1/2}$	$^2P_{3/2}$	$\Delta E^{(corr)}$
98	$18s, 18p, 9d, 6f, 4g, 3h$	-58.852	-64.185	5138.25
120	$20s, 20p, 11d, 8f, 6g, 5h$	-59.433	-65.183	5310.54
142	$22s, 22p, 13d, 10f, 8g, 7h$	-58.762	-64.461	5544.10
164	$24s, 24p, 15d, 12f, 10g, 9h$	-58.347	-63.985	5649.74
175	$25s, 25p, 16d, 13f, 11g, 10h$	-58.273	-63.896	5665.85
181	$27s, 27p, 16d, 13f, 11g, 10h$	-58.273	-63.896	5665.34
	In			
110	$18s, 18p, 13d, 6f, 5g, 4h$	-67.934	-87.128	4378.54
132	$20s, 20p, 15d, 8f, 7g, 6h$	-68.339	-87.489	4554.95
154	$22s, 22p, 17d, 10f, 9g, 8h$	-67.203	-86.093	4912.85
176	$24s, 24p, 19d, 12f, 11g, 10h$	-64.678	-82.842	5393.83
187	$25s, 25p, 20d, 13f, 12g, 11h$	-64.024	-82.036	5522.92
192	$26s, 26p, 21d, 13f, 12g, 11h$	-64.027	-81.996	5522.97
197	$27s, 27p, 22d, 13f, 12g, 11h$	-64.027	-81.996	5522.97

the effects of Breit interaction, vacuum polarization (VP), and the self-energy (SE) corrections in the basis set generation. For the Breit interaction, we employ the expression given in Ref. [37] and incorporate it at the level of orbital basis as well as the PRCC calculations. The effects of the vacuum polarization is considered using the Uehling potential [56], modified to incorporate the finite size effects of nucleus [57]. To compute the corrections from vacuum polarization to the single-electron energies we used the Uehling potential [56], with the modification to incorporate the finite-size effect of the nuclear charge distribution [57,58],

$$V_{\text{Ue}}(r) = -\frac{2\alpha}{3r} \int_0^\infty dx \, x\rho(x) \int_1^\infty dt \sqrt{t^2-1} \left(\frac{1}{t^3} + \frac{1}{2t^5} \right)$$
$$\times \left(e^{-2ct|(r-x)|} - e^{-2ct(r+x)} \right), \tag{33}$$

where α is the fine-structure constant and should not be confused with dipole polarizability. The nuclear charge density $\rho(x)$ is the finite-size Fermi density distribution

$$\rho_{\text{nuc}}(r) = \frac{\rho_0}{1 + e^{(r-c)/a}}, \tag{34}$$

with $a = t4\ln(3)$. The parameter c is the half charge radius such that $\rho_{\text{nuc}}(c) = \rho_0/2$, and t is the skin thickness. The self-energy corrections to single-electron energies are incorporated through the model Lamb-shift operator introduced by Shabaev *et al.* [59] and were calculated using the code QEDMOD [60].

Owing to the mathematically incomplete nature of the GTO basis [61], it is essential to check the convergence of properties with the basis size. In Table I we demonstrate the convergence of α for Al and In by listing α for both the fine-structure states as a function of the basis size. Similar data are also presented for the electron correlation energy for the ground state. For these calculations we have used the Dirac-Coulomb (DC) Hamiltonian as using the DCB Hamiltonian is computationally more expensive. As evident from the table, to achieve the convergence of α, we start with a moderate basis size by considering up to the h symmetry and
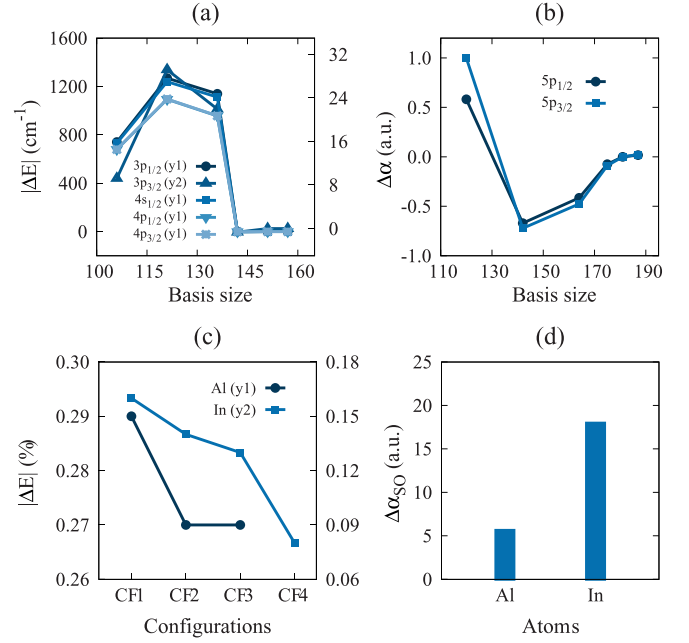

FIG. 14. Convergence of properties as a function of basis size for Al (a) excitation energies and (b) dipole polarizability. (c) Percentage change in the ground-state energies of Al and In. (d) Difference in the α values of spin-orbit split states, $^2P_{1/2}$ and $^2P_{3/2}$, of Al and In. In (a) and (c), the plot with labels $y1$ ($y2$) corresponds to the values indicated on the left (right) y axis.

then systematically increase the number of orbitals in each symmetry until the change in α is $\leqslant 10^{-3}$ a.u. For example, in the case of Al, the change in α is 2×10^{-8} a.u. when the basis set is augmented from 175 to 181 orbitals. So we consider the basis set with the 175 orbitals as the optimal set and use it in further calculations to incorporate the effects of the Breit interaction and QED corrections. The same approach is also adopted to achieve the convergence of excitation energies, however, with a key difference. In this case, the basis set includes orbitals from j symmetry also. The convergence trends of the excitation energies and α are shown in Figs. 14(a) and 14(b), respectively. As is discernible from the figure, both the excitation energy and α converge well with the basis size.

V. RESULTS AND DISCUSSION

A. Excitation energies

The excitation energy of a state $|\Psi_w\rangle$ is defined as

$$\Delta E_w = E_w - E_v, \tag{35}$$

where E_v is the energy of the ground-state wave function and obtained from the solution of Eq. (2) for $3p_{1/2}$ and $5p_{1/2}$ states for Al and In, respectively, and E_w is the energy of an excited state $|\Psi_w\rangle$. In the RCC E_w is given by [41]

$$E_w = \langle \Phi_w | \bar{H}^{\text{DCB}} (1 + S^{(0)}) | \Phi_w \rangle, \tag{36}$$

where $|\Phi_w\rangle$ is an excited Dirac-Fock state. In Table II we have listed the energy of the ground state and the excitation energies of a few low-lying states of Al and In. For comparison, the experimental values from NIST [62] are also listed in the table. For Al, our theoretical results are in excellent agreement

TABLE II. Energy (cm^{-1}) of the ground-state and the excitation energies of low-lying atomic states of Al and In calculated using RCC theory.

States	RCC results	NIST [62]
	Al	
$3s^2\,3p_{1/2}$	48 147.69	48 275.20
$3s^2\,3p_{3/2}$	111.93	112.06
$3s^2\,4s_{1/2}$	25 363.81	25 347.76
$3s^2\,4p_{1/2}$	32 927.34	32 949.81
$3s^2\,4p_{3/2}$	32 938.49	32 965.64
	In	
$5s^2\,5p_{1/2}$	46 633.75	46 670.20
$5s^2\,5p_{3/2}$	2411.59	2212.59
$5s^2\,6s_{1/2}$	24 413.48	24 372.96
$5s^2\,6p_{1/2}$	31 864.31	31 816.96
$5s^2\,6p_{3/2}$	32 179.48	32 115.22
$5s^2\,5d_{3/2}$	32 912.20	32 892.21
$5s^2\,5d_{5/2}$	32 921.59	32 915.54

with the experimental data for all states. The maximum relative error is 0.26%, in the case of the $3p_{1/2}$ state. For In also we observe the same trend of relative errors except for the state $5p_{3/2}$, where the error is 9%. This could be attributed to the correlation effects from higher energy configurations not included in the present work due to divergence issues.

To discern the electron correction effects as a function of configurations included in the computations, energies are computed with different configuration spaces in steps. For this we start with the ground-state configuration in the configuration space and include the higher energy configurations in subsequent steps. For Al, we start with $3s^23p$ and refer to this as CF1. Then we include two configurations $3s^24s$

and $3s^24p$ in two subsequent calculations (CF2 and CF3), respectively. The inclusion of the configuration $3s^23d$, however, leads to the divergence in the FSRCC computations due to the small energy denominator, and hence, we do not compute the excitation energy of $3d$. For In, $5s^25p$ (CF1) is the starting configuration, and the excited state configurations $5s^26s$, $5s^26p$, and $5s^25d$ are included in the later computations with configuration spaces identified as CF2, CF3, and CF4, respectively. The trend of contributions from the higher energy configurations to the ground-state energies of Al and In is shown in Fig. 14(c). As we observe from the figure, for both atoms, the relative error decreases with the inclusion of higher energy configurations. The reason for this is attributed to the better inclusion of the *core-valence* and *valence-valence* correlations with larger configuration space.

B. Polarizability

The values of α for the ground state, $^2P_{1/2}$, and the SO-coupled excited state, $^2P_{3/2}$, are listed in Tables III and IV, respectively. For comparison the other theoretical and experimental results from the previous works are also included. In the tables the results listed as PRCC are using the DC Hamiltonian and the converged bases with orbitals $25s25p16d13f11g10h$ and $26s26p21d13f12g11h$ for Al and In, respectively, and the results listed as PRCC+Breit+QED incorporate the effects of Breit and QED corrections. The values listed as *estimated* refer to the value after incorporating the estimated contributions from the i-, j-, and k-symmetry orbitals. The contributions from the DF and LPRCC are listed separately to assess the electron correlations effects subsumed by the nonlinear terms in the PRCC.

From the tables, we observe three important trends in the DF, LPRCC, and PRCC α results of Al and In. First, except for the $^2P_{3/2}$ state of In, the LPRCC results are lower than

TABLE III. The value of α (a.u.) for the $^2P_{1/2}$ state from the present work using PRCC and those reported in previous work.

Present work		Previous work	
Results	Method	Results	Method
		Al	
57.083	DF	55.4 ± 2.2 [20]	Multi-reference configuration interaction (MRCI)
51.537	LPRCC	57.74 [23]	Coupled-cluster single-double with partial triples [CCSD(T)]
58.273	PRCC	57.8 ± 1.0 [22]	State-interacting spin-orbit configuration interaction (SI-SOCI)
58.391	PRCC(T)	58.0 ± 0.4 [24]	Coupled-cluster single-double with partial triples [CCSD(T)]
58.808	PRCC(T)+Br.	61.0 [25]	Density functional theory with self-interaction correction (SIC_DFT)
58.808	PRCC(T)+Br.+QED	46 ± 2 [26]	Exp.
58.814	Est.	55.3 ± 5.5 [27]	Exp.
58.81(118)	Reco.		
		In	
62.756	DF	61.9 ± 1.2 [20]	Multi-reference configuration interaction (MRCI)
58.544	LPRCC	62.0 ± 1.9 [21]	Fock-space coupled-cluster with partial triples [FSCC(T)]
64.027	PRCC	61.5 ± 5.6 [63]	Coupled-cluster single-double with partial triples [CCSD(T)]
64.098	PRCC(T)	66.4 ± 5.0 [22]	State-interacting spin-orbit configuration interaction (SI-SOCI)
64.317	PRCC(T)+Br.	70.3 [25]	Density functional theory with self-interaction correction (SIC_DFT)
64.340	PRCC(T)+Br.+QED	68.7 ± 8.1 [28]	Exp.
64.299	Est.	62.1 ± 6.1 [29]	Exp.
64.30(129)	Reco.		

TABLE IV. The value of α (a.u.) for the $^2P_{3/2}$ state from the present work using PRCC and those reported in previous work.

Present work		Previous work	
Results	Method	Results	Method
	Al		
57.655	DF	55.9 ± 2.2 [20]	MRCI
57.421	LPRCC	58.0 ± 1.0 [22]	SI-SOCI
63.896	PRCC		
63.885	PRCC(T)		
64.692	PRCC(T)+Br.		
64.693	PRCC(T)+Br.+QED		
64.682	Est.		
64.68(129)	Reco.		
	In		
76.157	DF	69.7 ± 1.4 [20]	MRCI
76.586	LPRCC	74.4 ± 8.0 [22]	SI-SOCI
81.996	PRCC	69.6 ± 3.5 [21]	FSCC(T)
81.760	PRCC(T)		
82.309	PRCC(T)+Br.		
82.257	PRCC(T)+Br.+QED		
82.264	Est.		
82.26(165)	Reco.		

the DF results. This could be attributed to the contraction of the core with the inclusion of correlation effects within the LPRCC. Second, for both atoms the PRCC values are larger than the DF. This is due to the contribution of electron correlations from the nonlinear terms. In particular, we find the contributions from the nonlinear terms with one each of the perturbed and unperturbed CC operators, *viz.*, $\overline{H_N \mathbf{T}^{(1)}} S^{(0)}$ and $\overline{H_N T^{(0)}} \mathbf{S}^{(1)}$, are most prominent. And, third, the difference between the α of the fine-structure states, α_{FS}, of In is more than three times larger than Al. This is shown in Fig. 14(d). The reason for this could be the larger difference in the radial extents of the $^2P_{1/2}$ and $^2P_{3/2}$ states in In. In the DF results, $\langle r \rangle_{^2P_{3/2}} - \langle r \rangle_{^2P_{1/2}} = 0.138$ a.u. for In; however, it is only 0.007 a.u. for Al.

1. $^2P_{1/2}$

For the $^2P_{1/2}$ state of Al, there are two experimental results of α. However, the reported results have a large difference. The latest experimental result of α given in Ref. [27] is $\approx 20\%$ larger than the previous result reported in Ref. [26]. More importantly, there is a significant difference in the experimental errors. The measurement in Ref. [27] has an experimental error of $\approx 10\%$, whereas in Ref. [26] it is $\approx 4\%$. Our recommended value of 58.70 is $\approx 6\%$ larger than Ref. [27]. As listed in the table there are five theoretical results from previous works. These include two coupled-cluster results, similar to the method we have employed in the present work, but with a key difference in the computation of α. The two previous works used a finite-field method. Like in the experimental results, here as well, there is a wide variation in the reported values. There is a difference of about 10% between the lowest [20] and the highest [25] reported values. Although Refs. [20] and [22] adopt the same quantum many-body method, the

value in Ref. [22] is larger than Ref. [20]. Our PRCC value of 58.27 is in good agreement with the CCSD(T) results reported in Refs. [23] and [24] and the SI-SOCI result [22]. However, our recommended value 58.70 is on the higher side of these results. The reason for this is attributed to the inclusion of the contributions from the Breit and QED corrections and the large basis sets in our calculations.

For In also there are two experimental results for ground state, and, like in Al, there is a large difference between the two results. The recent measurement using the molecular-beam electric deflection technique [29] is about 10.6% larger in value than the result in Ref. [28]. Our recommended value 64.23 lies between the two results. Among the previous theoretical results, in terms of methods adopted, the results from Borschevsky *et al.* [21] and Safronova *et al.* [63] are in good agreement with our results. Considering uncertainties, our recommended value 64.23 is in good agreement with the previous results. The reason for a small difference could be attributed to the difference in the basis set and the contributions from the Breit and QED corrections. The other two results are using the CI-based methods. The result of 66.4 from Ref. [22] is the largest among all the results and differs by about 8% from the smallest value 61.5, Ref. [20].

2. $^2P_{3/2}$

The static dipole polarizability of the $^2P_{3/2}$ state, unlike the $^2P_{1/2}$ state, has contributions from the anisotropy components associated with magnetic quantum numbers $M_J = \pm 3/2$ and $\pm 1/2$. In Table IV we have given the final value of α from our calculation and compare with the previous theory results. Analyzing the results we observe three important differences in the trend of the electron correlation effects in comparison with the $^2P_{1/2}$ state. First, for both atoms, the DF and LPRCC results have similar values. This indicates there is less contraction of the core orbitals with the inclusion of correlation effects. Second, the percentage contribution from the nonlinear terms in PRCC is less than $^2P_{1/2}$. And, third, the overall Breit+QED correction is twice larger.

To the best of our knowledge, for both the atoms, there are no experimental results of α for the $^2P_{3/2}$ state, and among the previous results only a few are based on relativistic calculations. In Refs. [20] and [21], the coupled-cluster method is employed to obtain the energy of Al and In, respectively, and then α is computed using the finite-field approach. In Ref. [22], however, the configuration interaction method is combined with the finite-field approach to calculate the α. For Al, our LPRCC result is within the theoretical uncertainty of Refs. [20,22]. There is, however, an important difference from Refs. [20,22]. The value of α reported from our calculation is independent of M_J, as it is calculated in terms of reduced matrix elements. The values reported from Refs. [20,22], however, are the average of the α for two M_J values. A similar trend is observed in the case of In as well; that is, our LPRCC results are in agreement with the values reported in the previous works [20–22]. Our recommended values are larger than the values in Refs. [20,21]. From the detailed analysis of correlation effects in α for $^2P_{3/2}$, we find the reason for the larger value of α is the large core-polarization (CP) and valence-virtual correlation (VC) effects. As discussed in the

TABLE V. Contributions to α (a.u.) from different terms in PRCC theory for Al and In.

| Terms + H.c.	Al		In	
	$^2P_{1/2}$	$^2P_{3/2}$	$^2P_{1/2}$	$^2P_{3/2}$
$\mathbf{S}^{(1)\dagger}\mathbf{D}$	85.3337	88.4131	90.0421	107.8206
$\mathbf{S}^{(1)\dagger}\mathbf{D}S^{(0)}$	−9.1048	−5.7448	−12.2584	−11.7265
$T^{(0)\dagger}\mathbf{D}\mathbf{S}^{(1)}$	−1.8365	−2.2499	−0.7316	−0.9715
$S^{(0)\dagger}\mathbf{D}\mathbf{T}^{(1)}$	−7.2333	−7.2820	−5.5342	−5.5331
$\mathbf{T}^{(1)\dagger}\mathbf{D}$	−7.6424	−7.9950	−7.4631	−7.1608
$T^{(0)\dagger}\mathbf{D}\mathbf{T}^{(1)}$	0.9567	1.1739	1.5013	1.5164
Normalization	−0.9636	−0.9744	−0.9767	−0.9768
Total	58.2732	63.8955	64.0271	81.9959

next section, besides DF, these are the other important contributions and these are accounted accurately in our computation through the PRCC terms $\mathbf{DS}_1^{(1)}$ + H.c. and $\mathbf{DS}_2^{(1)}$ + H.c. A sizable contribution from the Breit interaction and QED corrections is also observed. Our recommended value 82.50 is within the theoretical uncertainty of Ref. [22].

C. Electron correlations

Next, we analyze and present the different electron correlations effects incorporated in the calculations of α. For this, we separate the expression in Eq. (31) into six different terms and give their contributions in Table V. As evident from the table, for both the atoms, the leading order (LO) term is $\mathbf{S}^{(1)\dagger}\mathbf{D}$ + H.c. The contribution from the LO term is $\approx$146%(138%) and $\approx$141%(131%) of the PRCC value for the $^2P_{1/2}(^2P_{3/2})$ state of Al and In, respectively; that is, the contribution from the LO term exceeds the total value. This is expected as it incorporates the results from the DF term and CP effects. Except for the $^2P_{3/2}$ of Al, the next leading order (NLO) term is $\mathbf{S}^{(1)\dagger}\mathbf{D}S^{(0)}$ + H.c. It contributes $\approx$ −10.6%(−6.5%) and −13.6%(−10.8%) for the $^2P_{1/2}(^2P_{3/2})$ state of Al and In, respectively. For the next to NLO contribution, the terms $\mathbf{S}^{(1)\dagger}\mathbf{D}S^{(0)}$ + H.c. and $\mathbf{T}^{(1)\dagger}\mathbf{D}$ + H.c. give nearly equal contributions. Like the NLO term, the contributions from these terms are opposite in phase to the LO contribution and, hence, reduce the total value of α. It is to be mentioned here that the contributions from the core electrons to α are important. This is unlike the properties of one-valence systems without an external perturbation like the electromagnetic transitions. This is reflected in the contribution from the term $\mathbf{T}^{(1)\dagger}\mathbf{D}$ + H.c. for both atoms.

1. Dominant contributions

To gain insights into the dominant contributions from the virtual orbitals, we compute α using basis sets with selective addition of orbitals in d-, f-, and g-symmetries; the results are plotted in Fig. 15. For Al the dominant contribution, as discernible from the figure, is from the d-virtual orbitals. A similar trend in Al$^+$ was reported in our previous work [31]. The same trend is also observed for In, but with a key difference. In this case the f orbitals also contribute, and this is consistent with the trend reported in our previous work [31], where the f-virtual electrons were found to have dominant
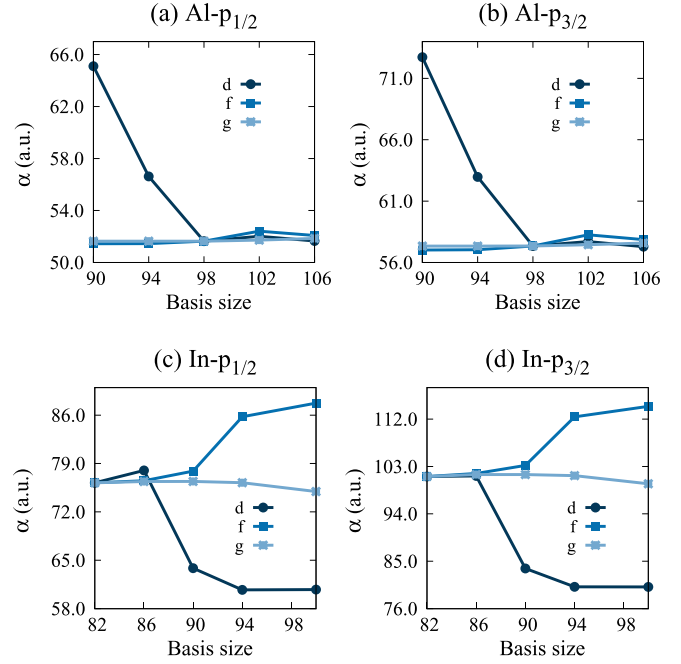
FIG. 15. Trend of contributions to α from virtual orbitals for Al (a, b) and In (c, d) as basis is augmented.

contribution due to strong dipolar mixing with the core electrons in the $4d$ orbital.

To quantify the orbital wise contributions, we identify the dominant cluster amplitudes which contribute to the LO term $\mathbf{DS}_1^{(1)}$ + H.c. As discernible from Fig. 17 below, for Al, at 40.9% (36.6%) the cluster operators with the virtual orbital $3d_{3/2}(3d_{5/2})$ have the largest contribution to the $^2P_{1/2}(^2P_{3/2})$ polarizability, due to the strong dipolar mixing between the $3p$ and $3d$ orbitals. The second largest contribution is observed from the cluster amplitudes with the $4s_{1/2}$ virtual orbital; the contribution is $\approx$25.3% (24.6%) for the $^2P_{1/2}(^2P_{3/2})$ state. The next three dominant contributions are from the $4d$, $8d$, and $7d$ virtual orbitals, and together they contribute $\approx$22.15% (20.18%) for the $^2P_{1/2}(^2P_{3/2})$ state. A similar trend is also observed in the case of In, where the first two dominant contributions are from the $5d$ and $6s$ orbitals. They contribute $\approx$38.7% (35.6%) and 25.6% (27.6%), respectively, for the $^2P_{1/2}(^2P_{3/2})$ state. In contrast to Al, the third and fourth dominant contributions are of the same order, and different d electrons contribute to $^2P_{1/2}$ and $^2P_{3/2}$ states.
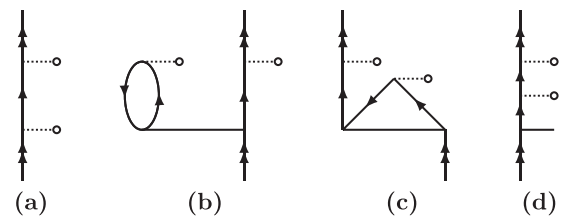
FIG. 16. The DF (a), CP (b, c), and VC (d) terms subsumed in $DS_1^{(1)}$.

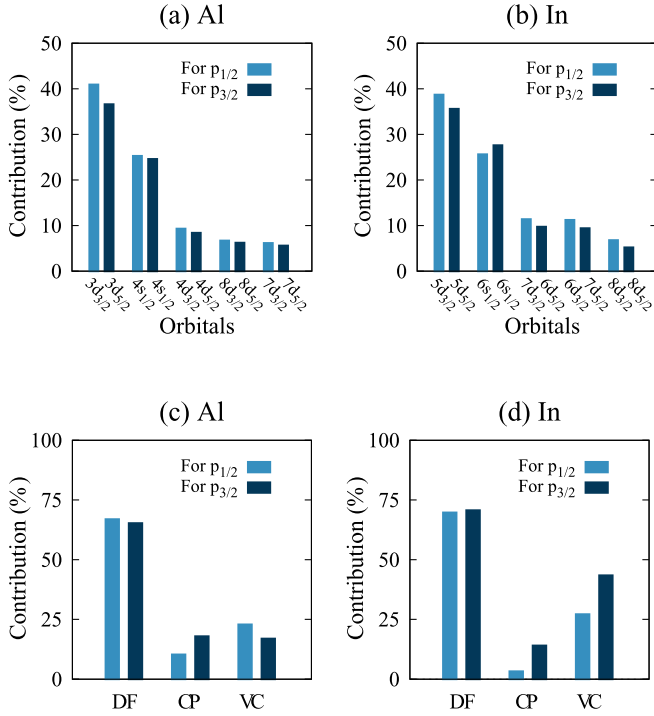FIG. 17. Five largest percentage contributions to $DS_1^{(1)}$ + H.c. for $^2P_{1/2}$ and $^2P_{3/2}$ states of Al (a) and In (b). The percentage contributions from DF, CP, and VC for Al (c) and In (d).

2. Core polarization, valence-virtual correlation, QED effects, and perturbative triples

Next we assess the contributions from core-polarization and pair-correlation effects to α of Al and In. The term $\mathbf{DS}_1^{(1)}$ subsumes the contributions from DF, core-polarization, and valence-virtual correlation effects. The diagrams contributing to these are shown in Fig. 16. The other dominant contribution to the core polarization is from the term $\mathbf{DS}_2^{(1)}$, and the corresponding diagram is shown in Fig. 10(b) and its exchange. The contribution from the valence-virtual correlation is estimated by subtracting the contributions of Figs. 16(a), 16(b), and 16(c) from $\mathbf{DS}^{(1)}$. The percentage contributions of DF, CP, and VC are shown in Fig. 17.

For both atoms, as to be expected, the DF has the largest contribution. In terms of percentage, it constitutes $\approx 66.9\%$ (65.2%) and 69.7% (70.6%) of the $\mathbf{DS}^{(1)}$ contribution for the $^2P_{1/2}$($^2P_{3/2}$) state of Al and In, respectively. Between CP and VC, except for the $^2P_{3/2}$ state of Al, the contribution from VC effect is larger than CP, and it is more significant in the case of In. In quantitative terms, it constitutes $\approx 22.8\%$ (16.9%) and 27.1% (43.4%) of the $\mathbf{DS}^{(1)}$ for the $^2P_{1/2}$($^2P_{3/2}$) state of Al and In, respectively. The CP contributions are $\approx 10.3\%$ (17.9%) and 3.2% (13.9%) of the $\mathbf{DS}^{(1)}$ for the $^2P_{1/2}$($^2P_{3/2}$) state of Al and In. It is, however, to be emphasized that the CP contribution in In is smaller than Al. This indicates a better screening of nuclear potential in In. The VC contribution, on the contrary, is larger than Al. Further, as is discernible from Fig. 17, except for VC in Al, the CP and VC effects are larger in $^2P_{3/2}$. For example, for the $^2P_{3/2}$ state of In, the CP contribution is 4.4 times larger than $^2P_{1/2}$. Similarly, the VC contribution is 1.6 times that of $^2P_{1/2}$. This naturally leads to

TABLE VI. Contributions to α (a.u.) from Breit interaction, vacuum polarization, and self-energy corrections from PRCC calculation.

	Al		In	
	$^2P_{1/2}$	$^2P_{3/2}$	$^2P_{1/2}$	$^2P_{3/2}$
DC	58.2732	63.8955	64.0272	81.9959
Breit	0.4172	0.8072	0.2192	0.5490
Self-energy	−0.0012	−0.0002	0.0025	−0.0380
Vacuum polarization	0.0013	0.0013	0.0205	−0.0139

a larger α for the $^2P_{3/2}$ state, for both atoms, when compared to the previously reported values.

The contributions from the Breit interaction, vacuum polarization, and self-energy corrections are listed in Table VI, and, for easy comparison, the contributions in percentage are plotted in Fig. 18. As is discernible from the figure, for both states, the Breit contribution in Al is larger than In. This is consistent with the trend reported in our previous work [31] where we found that, among all the group-13 ions, Al$^+$ has the highest contribution. The largest contribution is $\approx 1.3\%$ for the $^2P_{3/2}$ state. For the VP and SE contributions, in contrast to the trend of Breit contribution, these are larger in In than Al. The largest contribution from VP is $\approx 0.3\%$ for the $^2P_{1/2}$ state, whereas SE has the largest contribution of $\approx 0.5\%$, for the case of the $^2P_{3/2}$ state of In. The largest combined contribution from Breit interaction and QED corrections is $\approx 1.3\%$, in the case of the $^2P_{3/2}$ state of Al. Considering the need of accurate α from theory calculations, this is a significant contribution and cannot be ignored.

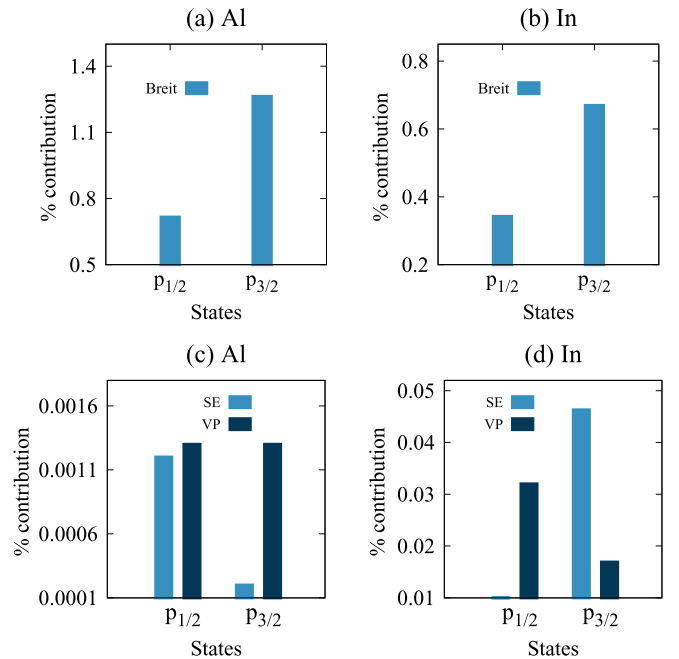

FIG. 18. Contributions from the Breit interaction, vacuum polarization, and self-energy corrections for $^2P_{1/2}$ and $^2P_{3/2}$ states of Al and In.

TABLE VII. Contributions from the p-p and h-h types of perturbative triples arising from $S^{(0)\dagger}\mathbf{D}g\mathbf{S_2^{(1)}}$ and $S^{(0)\dagger}\mathbf{D}g\mathbf{T_2^{(1)}}$ terms.

	Al		In	
Terms + H.c.	$^2P_{1/2}$	$^2P_{3/2}$	$^2P_{1/2}$	$^2P_{3/2}$
$S^{(0)\dagger}\mathbf{D}g\mathbf{S_2^{(1)}}$ (p-p)	0.0935	0.0616	0.0872	0.0986
(h-h)	0.0039	−0.0008	0.0031	−0.0020
$S^{(0)\dagger}\mathbf{D}g\mathbf{T_2^{(1)}}$ (p-p)	−0.02744	−0.08247	−0.01090	−0.34036
(h-h)	−0.02381	0.01028	−0.00865	0.00739
Total	0.04615	−0.01139	0.07075	−0.23637

The contributions from the perturbative triples are listed in Table VII. On closer inspection of the table, we observe that the contribution from $S^{(0)\dagger}\mathbf{D}g\mathbf{T_2^{(1)}}$ is opposite in phase to $S^{(0)\dagger}\mathbf{D}g\mathbf{S_2^{(1)}}$ for both p-p and h-h group of diagrams. This leads to the cancellation and reduces the total contribution from perturbative triples. The other important observation from the table is that the $^2P_{3/2}$ state has negative contribution for both atoms. The largest contribution of $\approx 0.3\%$ of PRCC values is observed, in the case of the $^2P_{3/2}$ state of In.

D. Theoretical uncertainty

Based on the various approximations used in the computations of α, we have identified four sources of uncertainties. The first source of uncertainty is associated with the basis set truncation. From the convergence of α we observe that the change in α, with orbitals up to h symmetry, is $\leqslant 10^{-3}$ (a.u.) when the optimal basis set is augmented, and, as listed in Table IV, the largest overall contribution from the i, j, and k symmetry orbitals is in the case of $^2P_{3/2}$ of In and amounts to $\approx 0.06\%$. Although the combined contribution from the orbitals with higher symmetries, beyond the k symmetry, is expected to be smaller, we take 0.1% as an upper bound from this source. The second source of uncertainty is the truncation of the dressed operator $\bar{\mathbf{D}}$ to $\mathbf{D} + \mathbf{D}T^{(0)} + T^{(0)\dagger}\mathbf{D} + T^{(0)\dagger}\mathbf{D}T^{(0)}$. To estimate the uncertainty from this source, we use the findings from our previous work [41] where we showed that the terms with third order in $T^{(0)}$ and higher together contribute less than 0.1%. We take this as the upper bound from this source. The third source of uncertainty is the truncation of CC operators to singles and doubles. Among the higher excitations, triple excitations contribute the most, and the dominant contribution is subsumed in the perturbative triples. Therefore, in the present work we have included the contributions from the perturbative triples arising from $S^{(0)\dagger}\mathbf{D}g\mathbf{S_2^{(1)}}$ and $S^{(0)\dagger}\mathbf{D}g\mathbf{T_2^{(1)}}$. Based on the analysis of the contributions to α from the CC terms at the CCSD level, these are expected to have dominant contributions. We observed the largest contribution of 0.3%, in the case of the $^2P_{3/2}$ state of In. This is consistent with the observed largest contribution of 0.28% for In$^+$ in our previous work [31]. So, from this source of uncertainty we take 1.0% as an upper bound for the cumulative contribution from the missing correlation effects in perturbative triples and higher excitations and their basis dependence. The last source of theoretical uncertainty is associated with the frequency-dependent Breit interaction,

which is not included in our calculations. To estimate an upper bound of this source we use the results in our previous work [64], where using GRASP2K we estimated an upper bound of 0.13% for Ra. As Al and In are lighter than Ra, the contribution is expected to be smaller, and we take 0.13% as the uncertainty from this source. There could be other sources of theoretical uncertainties, such as the higher order coupled perturbation of vacuum polarization and self-energy terms, etc. These, however, have much smaller contributions, and their combined uncertainty could be below 0.1%. Combining the upper bounds of all four sources of uncertainties, we estimate a maximum theoretical uncertainty of 2% in the recommended value of α.

VI. CONCLUSION

We have developed a relativistic coupled-cluster theory-based method to compute the properties of one-valence atoms and ions with an external perturbation. We employ this method to calculate the electric dipole polarizability of ground state and SO-split excited state of Al and In. In addition, to test the quality of the wave functions, we also calculated the excitation energy of few low-lying states. To improve the accuracy of α further, contributions from the Breit interaction and QED corrections are included, and, to ensure the convergence of α with basis size, large bases up to k-symmetry are used.

For the $^2P_{1/2}$ state, our recommended value lies within the range of the previous theoretical results for both atoms. In particular, our results are closer to those reported in Refs. [22] and [21] for Al and In, respectively. For the $^2P_{3/2}$ state, however, our recommended value is lager than the previous values. It is to be mentioned that our LPRCC values are closer to the previous results. The reason for the larger PRCC values could be attributed to better inclusion of correlation effects through the inclusion of nonlinear terms.

From the analysis of the electron correlations, we find that for both atoms, the VC contribution is larger than CP. Between Al and In, the contribution from CP decreases, but VC effects are found to increase. In terms of orbital contributions, for Al, the first two dominant contributions to α come from the $3p$-$3d$ and $3p$-$4s$ dipolar mixings. For In, however, they are from the $5p$-$5d$ and $5p$-$6s$ mixings. For the contribution from the Breit interaction, the largest contribution is $\approx 1.3\%$ of the DC value, observed in the case of the $^2P_{3/2}$ state of Al. The largest contributions from the Uehling potential and the self-energy corrections are $\approx 0.3\%$ and 0.5%, respectively, in the case of $^2P_{1/2}$ and $^2P_{3/2}$ states of In.

[1] H. G. Dehmelt, Mono-ion oscillator as potential ultimate laser frequency standard, IEEE Trans. Instrum. Meas. **IM-31**, 83 (1982).

[2] C. W. Chou, D. B. Hume, J. C. J. Koelemeij, D. J. Wineland, and T. Rosenband, Frequency Comparison of Two High-Accuracy Al$^+$ Optical Clocks, Phys. Rev. Lett. **104**, 070802 (2010).

[3] M. S. Safronova, M. G. Kozlov, and C. W. Clark, Precision Calculation of Blackbody Radiation Shifts for Optical Frequency Metrology, Phys. Rev. Lett. **107**, 143006 (2011).

[4] Z. Zuhrianda, M. S. Safronova, and M. G. Kozlov, Anomalously small blackbody radiation shift in the Tl$^+$ frequency standard, Phys. Rev. A **85**, 022513 (2012).

[5] J.-S. Chen, S. M. Brewer, C. W. Chou, D. J. Wineland, D. R. Leibrandt, and D. B. Hume, Sympathetic Ground State Cooling and Time-Dilation Shifts in an ^{27}Al$^+$ Optical Clock, Phys. Rev. Lett. **118**, 053002 (2017).

[6] S. M. Brewer, J.-S. Chen, A. M. Hankin, E. R. Clements, C. W. Chou, D. J. Wineland, D. B. Hume, and D. R. Leibrandt, ^{27}Al$^+$ Quantum-Logic Clock with a Systematic Uncertainty Below 10^{-18}, Phys. Rev. Lett. **123**, 033201 (2019).

[7] S. M. Brewer, J.-S. Chen, K. Beloy, A. M. Hankin, E. R. Clements, C. W. Chou, W. F. McGrew, X. Zhang, R. J. Fasano, D. Nicolodi, *et al.*, Measurements of ^{27}Al$^+$ and ^{25}Mg$^+$ magnetic constants for improved ion-clock accuracy, Phys. Rev. A **100**, 013409 (2019).

[8] W. A. van Wijngaarden, Precision measurements of atomic polarizabilities, in *The Sixteenth International Conference on Atomic Physics*, edited by W. E. Baylis and G. W. F. Drake, AIP Conf. Proc. No. 477 (AIP, New York, 1999), p. 305.

[9] I. B. Khriplovich, *Parity Nonconservation in Atomic Phenomena* (Gordon and Breach, Philadelphia, 1991).

[10] W. C. Griffith, M. D. Swallows, T. H. Loftus, M. V. Romalis, B. R. Heckel, and E. N. Fortson, Improved Limit on the Permanent Electric Dipole Moment of Hg^{199}, Phys. Rev. Lett. **102**, 101601 (2009).

[11] M. H. Anderson, J. R. Ensher, M. R. Matthews, C. E. Wieman, and E. A. Cornell, Observation of Bose-Einstein condensation in a dilute atomic vapor, Science **269**, 198 (1995).

[12] C. C. Bradley, C. A. Sackett, J. J. Tollett, and R. G. Hulet, Evidence of Bose-Einstein Condensation in an Atomic Gas with Attractive Interactions, Phys. Rev. Lett. **75**, 1687 (1995).

[13] K. B. Davis, M. O. Mewes, M. R. Andrews, N. J. van Druten, D. S. Durfee, D. M. Kurn, and W. Ketterle, Bose-Einstein Condensation in a Gas of Sodium Atoms, Phys. Rev. Lett. **75**, 3969 (1995).

[14] M. Lewenstein, Ph. Balcou, M. Yu. Ivanov, A. L'Huillier, and P. B. Corkum, Theory of high-harmonic generation by low-frequency laser fields, Phys. Rev. A **49**, 2117 (1994).

[15] M. Lewenstein, P. Salières, and A. L'Huillier, Phase of the atomic polarization in high-order harmonic generation, Phys. Rev. A **52**, 4747 (1995).

[16] C. I. Blaga, F. Catoire, P. Colosimo, G. G. Paulus, H. G. Muller, P. Agostini, and L. F. DiMauro, Strong-field photoionization revisited, Nat. Phys. **5**, 335 (2009).

[17] Y. H. Lai, C. I. Blaga, J. Xu, H. Fuest, P. Rupp, M. F. Kling, P. Agostini, and L. F. DiMauro, Polarizability effect in strong-field ionization: Quenching of the low-energy structure in C$_{60}$, Phys. Rev. A **98**, 063427 (2018).

[18] S. G. Karshenboim and E Peik, *Astrophysics, Clocks and Fundamental Constants*, Lecture Notes in Physics Vol. 648 (Springer, New York, 2010).

[19] M. T. Murphy, J. K. Webb, and V. V. Flambaum, Comment on "Limits on the Time Variation of the Electromagnetic Fine-Structure Constant in the Low Energy Limit from Absorption Lines in the Spectra of Distant Quasars", Phys. Rev. Lett. **99**, 239001 (2007).

[20] T. Fleig, Spin-orbit-resolved static polarizabilities of group-13 atoms: Four-component relativistic configuration interaction and coupled cluster calculations, Phys. Rev. A **72**, 052506 (2005).

[21] A. Borschevsky, T. Zelovich, E. Eliav, and U. Kaldor, Precision of calculated static polarizabilities: Ga, In and Tl atoms, Chem. Phys. **395**, 104 (2012).

[22] A. A. Buchachenko, State-interacting spin-orbit configuration interaction method for J-resolved anisotropic static dipole polarizabilities: Application to Al, Ga, In, and Tl atoms, Russian J. Phys. Chem. A **84**, 2325 (2010).

[23] C. Lupinetti and A. J. Thakkar, Polarizabilities and hyperpolarizabilities for the atoms Al, Si, P, S, Cl, and Ar: Coupled cluster calculations, J. Chem. Phys. **122**, 044301 (2005).

[24] P. Fuentealba, The static dipole polarizability of aluminium atom: Discrepancy between theory and experiment, Chem. Phys. Lett. **397**, 459 (2004).

[25] X. Chu and A. Dalgarno, Linear response time-dependent density functional theory for van der Waals coefficients, J. Chem. Phys. **121**, 4083 (2004).

[26] P. Milani, I. Moullet, and W. A. de Heer, Experimental and theoretical electric dipole polarizabilities of Al and Al$_2$, Phys. Rev. A **42**, 5150 (1990).

[27] G. S. Sarkisov, I. L. Beigman, V. P. Shevelko, and K. W. Struve, Interferometric measurements of dynamic polarizabilities for metal atoms using electrically exploding wires in vacuum, Phys. Rev. A **73**, 042501 (2006).

[28] T. P. Guella, Thomas M. Miller, B. Bederson, J. A. D. Stockdale, and B. Jaduszliwer, Polarizability of $5s^2 5p(^2 p_{\frac{1}{2}})$ atomic indium, Phys. Rev. A **29**, 2977 (1984).

[29] L. Ma, J. Indergaard, B. Zhang, I. Larkin, R. Moro, and W. A. de Heer, Measured atomic ground-state polarizabilities of 35 metallic elements, Phys. Rev. A **91**, 010501(R) (2015).

[30] B. K. Mani, S. Chattopadhyay, and D. Angom, Rccpac: A parallel relativistic coupled-cluster program for closed-shell and one-valence atoms and ions in FORTRAN, Comput. Phys. Commun. **213**, 136 (2017).

[31] R. Kumar, S. Chattopadhyay, B. K. Mani, and D. Angom, Electric dipole polarizability of group-13 ions using perturbed relativistic coupled-cluster theory: Importance of nonlinear terms, Phys. Rev. A **101**, 012503 (2020).

[32] R. Kumar, S. Chattopadhyay, D. Angom, and B. K. Mani, Fock-space relativistic coupled-cluster calculation of a hyperfine-induced $^1S_0 \rightarrow {}^3P_0^o$ clock transition in Al$^+$, Phys. Rev. A **103**, 022801 (2021).

[33] M. S. Safronova, W. R. Johnson, and A. Derevianko, Relativistic many-body calculations of energy levels, hyperfine constants, electric-dipole matrix elements, and static polarizabilities for alkali-metal atoms, Phys. Rev. A **60**, 4476 (1999).

[34] A. Derevianko, W. R. Johnson, M. S. Safronova, and J. F. Babb, High-Precision Calculations of Dispersion Coefficients, Static

Dipole Polarizabilities, and Atom-Wall Interaction Constants for Alkali-Metal Atoms, Phys. Rev. Lett. **82**, 3589 (1999).

[35] J. Mitroy, M. S. Safronova, and C. W. Clark, Theory and applications of atomic and ionic polarizabilities, J. Phys. B: At., Mol. Opt. Phys. **43**, 202001 (2010).

[36] P. Schwerdtfeger and J. K. Nagle, 2018 table of static dipole polarizabilities of the neutral elements in the periodic table, Mol. Phys. **117**, 1200 (2019).

[37] I. P. Grant and B. J. McKenzie, The transverse electron-electron interaction in atomic structure calculations, J. Phys. B **13**, 2671 (1980).

[38] A. K. Mohanty, F. A. Parpia, and E. Clementi, Kinetically balanced geometric Gaussian basis set calculations for relativistic many-electron atoms, in *Modern Techniques in Computational Chemistry: MOTECC-91*, edited by E. Clementi (ESCOM, Leiden, 1991), p. 167.

[39] R. E. Stanton and S. Havriliak, Kinetic balance: A partial solution to the problem of variational safety in Dirac calculations, J. Chem. Phys. **81**, 1910 (1984).

[40] B. K. Mani, K. V. P. Latha, and D. Angom, Relativistic coupled-cluster calculations of ^{20}Ne, ^{40}Ar, ^{84}Kr, and ^{129}Xe: Correlation energies and dipole polarizabilities, Phys. Rev. A **80**, 062505 (2009).

[41] B. K. Mani and D. Angom, Atomic properties calculated by relativistic coupled-cluster theory without truncation: Hyperfine constants of Mg$^+$, Ca$^+$, Sr$^+$, and Ba$^+$, Phys. Rev. A **81**, 042514 (2010).

[42] S. Chattopadhyay, B. K. Mani, and D. Angom, Perturbed coupled-cluster theory to calculate dipole polarizabilities of closed-shell systems: Application to Ar, Kr, Xe, and Rn, Phys. Rev. A **86**, 062508 (2012).

[43] P. Pulay, Convergence acceleration of iterative sequences. The case of scf iteration, Chem. Phys. Lett. **73**, 393 (1980).

[44] S. Fritzsche, B. K. Mani, and D. Angom, Chapter 10A Computer-algebraic approach to the derivation of Feynman-Goldstone perturbation expansions for open-shell atoms and molecules, Adv. Quantum Chemistry **53**, 177 (2008).

[45] I. Lindgren and J. Morrison, *Atomic Many-Body Theory*, 2nd ed. (Springer, Berlin).

[46] I. Shavitt and R. J. Bartlett, *Many-Body Methods in Chemistry and Physics: MBPT and Coupled-Cluster Theory*, Cambridge Molecular Science (Cambridge University Press, Cambridge, 2009).

[47] J. Noga and M. Urban, On expectation value calculations of one-electron properties using the coupled cluster wave functions, Theor. Chim. Acta **73**, 291 (1988).

[48] O. Zatsarinny and C. Froese Fischer, DBSR-HF: A B-spline Dirac-Hartree-Fock program, Comput. Phys. Commun. **202**, 287 (2016).

[49] S. Salomonson and P. Öster, Solution of the pair equation using a finite discrete spectrum, Phys. Rev. A **40**, 5559 (1989).

[50] J. C. Slater, Atomic shielding constants, Phys. Rev. **36**, 57 (1930).

[51] E. L. Shirley and R. M. Martin, *GW* quasiparticle calculations in atoms, Phys. Rev. B **47**, 15404 (1993).

[52] http://dirac.chem.sdu.dk/basisarchives/dyall/index.html.

[53] S. Huzinaga, Basis sets for molecular calculations, Comput. Phys. Rep. **2**, 281 (1985).

[54] R. K. Chaudhuri, P. K. Panda, and B. P. Das, Hybrid approach to relativistic Gaussian basis functions: Theory and applications, Phys. Rev. A **59**, 1187 (1999).

[55] P. Jönsson, G. Gaigalas, J. Bieroń, C. Froese Fischer, and I. P. Grant, New version: Grasp2K relativistic atomic structure package, Comput. Phys. Commun. **184**, 2197 (2013).

[56] E. A. Uehling, Polarization effects in the positron theory, Phys. Rev. **48**, 55 (1935).

[57] L. Wayne Fullerton and G. A. Rinker, Accurate and efficient methods for the evaluation of vacuum-polarization potentials of order $z\alpha$ and $z\alpha^2$, Phys. Rev. A **13**, 1283 (1976).

[58] S. Klarsfeld, Analytical expressions for the evaluation of vacuum-polarization potentials in muonic atoms, Phys. Lett. B **66**, 86 (1977).

[59] V. M. Shabaev, I. I. Tupitsyn, and V. A. Yerokhin, Model operator approach to the Lamb shift calculations in relativistic many-electron atoms, Phys. Rev. A **88**, 012513 (2013).

[60] V. M. Shabaev, I. I. Tupitsyn, and V. A. Yerokhin, Qedmod: Fortran program for calculating the model Lamb-shift operator, Comput. Phys. Commun. **189**, 175 (2015).

[61] I. Grant, Relativistic atomic structure, in *Springer Handbook of Atomic, Molecular, and Optical Physics*, edited by G. Drake (Springer, New York, 2006), pp. 325–357.

[62] Nist atomic spectroscopic database, https://physics.nist.gov/PhysRefData/ASD/levels_form.html (2013).

[63] M. S. Safronova, U. I. Safronova, and S. G. Porsev, Polarizabilities, Stark shifts, and lifetimes of the In atom, Phys. Rev. A **87**, 032513 (2013).

[64] S. Chattopadhyay, B. K. Mani, and D. Angom, Electric dipole polarizability of alkaline-earth-metal atoms from perturbed relativistic coupled-cluster theory with triples, Phys. Rev. A **89**, 022506 (2014).